The Pennsylvania State University

The Graduate School

College of Engineering

THE EFFECT OF VARIABLE INITIAL UNCERTAINTY ON THE

PROBABILITY OF ASTEROID-EARTH COLLISIONS

A Thesis in

Aerospace Engineering

by

Christopher Polito

Submitted in Partial Fulfillment

of the Requirements

for the Degree of

Master of Science

May 2011

The thesis of Christopher Polito was reviewed and approved* by the following:

David B. Spencer
Associate Professor of Aerospace Engineering
Thesis Advisor

Robert G. Melton
Professor of Aerospace Engineering

George A. Lesieutre
Professor of Aerospace Engineering
Head of the Department of Aerospace Engineering

Abstract

An alternative to the conventional method for determining impact probability by an asteroid is presented that utilizes the positional uncertainty ellipsoid. This method is used commonly for Earth-orbiting satellite collision probability. In the scaling up process, the gravitational influence of one of the bodies in the collision is taken into account, namely that of the Earth. The restricted three-body problem is sufficient to provide a backdrop for the probability analysis, while making sure to note that the results are only hypothetical given a simplified dynamic model. Uncertainty is represented mathematically by the 3σ covariance matrix and is propagated into the future by a linear transformation involving the State Transition Matrix (STM). Encounter regions are defined as regions along the nominal trajectory of the asteroid where the propagated uncertainty encloses the Earth. These regions are not known a priori. Probability is then calculated by a triple integral of the probability density function (pdf) (a function of the covariance matrix) over the volume swept out by the Earth through the encounter region. This integral is achieved by, first, integrating the instantaneous pdf at each time step in the encounter region, and then by integrating the resulting probability, as a function of time, over its domain. The process from propagating the uncertainty along the nominal trajectory, finding the encounter regions and calculating probability is repeated in a Monte Carlo simulation that varies the initial uncertainty. The orientation of the initial uncertainty ellipsoid is held constant: aligned with the velocity vector, while the lengths of the three principal axes (in-track, normal, and out-of-plane) are varied in their respective relative ranges. The trend in probability calculated vs. initial uncertainty is then investigated. It is found that higher probabilities result from initial uncertainties that are tighter in all three directions. That is, higher probabilities result when the position of the asteroid is known initially with more accuracy. This is an expected result because probability should be a conservative estimate so that likely encounters are not overlooked. And with

advances in observational and analytical techniques, the initial positions of asteroids will inevitably become more accurate so that more conservative probabilities will be calculated in the future. However, it is also shown that this positive result stems from the uncertainty being very large initially, so that as the uncertainty decreases substantially, the trend will tend to reverse. This fact is not demonstrated because large uncertainties are required for this method to proceed. Suggestions for future work are given to combat these limitations. With this alternative, and the suggestions for improving it, probabilities of impact by an asteroid can be calculated that are comparable to current automated methods.

Table of Contents

List of Figures

List of Tables

Acknowledgments

The starting point of this thesis was from a suggestion by my advisor, David Spencer, who wanted to study the probability of impact between an asteroid and the Earth. Without his suggestion and interest in this line of research, I would never have pursued it to this end. His close attention to my work through our weekly meetings and many draft reviews greatly contributed to and improved the work. He also introduced me to Ken Chan at the Aerospace Corporation who spoke with me about his work on satellite collision probability. I am indebted to Ken's openness with me about his work and the sharing of supplementary material that I believe he produced just for me, which can be found in the Appendix.

I would also like to thank the other employees at the Aerospace Corporation who were given a preliminary presentation in relation to this thesis and whose feedback contributed to the development of the work. Specifically I would like to thank Tom Starchville and Ron Clifton.

I want to thank my parents whose support for the pursuit of these educational goals over the years has been invaluable. Without them, I would never have produced this work. I thank my father who helped to edit several papers and essays I have written, *except* this one, however, his feedback on those other works contributed to the writing of this thesis. Also, my grandfather, whose support has been immeasurable, made this possible. I would like to thank my uncle whose own interest in the subject contributed immensely to different avenues of research.

In a more tangential way, I would like to thank the instructors whose guidance over the years through the subjects they taught contributed greatly to my ability to follow this line of research. Specifically, I would like to thank Robert Melton, Joseph Horn, Joseph Cusumano, Mark Maughmer, Michael Micci, George Lesieutre, and David Spencer, among others.

I would like to thank my peers with whom I had many discussions about this work, specifically Jesse McTernan and Chris DeForce. Their additional point of view helped me gain perspective and address the important questions.

For the number of non-technical people who heard about this research from me

and who expressed their own interest in it, I thank you. You are too numerous to be named.

I apologize to anyone whose name I did not mention who feels they contributed significantly or minimally to this work, your contributions did not go unnoticed.

Dedication

To my parents.

Chapter 1

Introduction

This thesis presents a method for calculating the probability of collision between an asteroid and the Earth. The question of what this probability is for a given asteroid can be answered in a variety of different ways. One of these methods is being put to practical use in an automated system to search for possible impactors and utilizes the Line of Variations (LOV) as its primary analytical tool. (The method of Line of Variations is discussed in Section 1.2.1.) This thesis presents a method for determining impact probability by using the positional uncertainty ellipsoid as its primary analytical tool.

The method of impact probability determination that is presented here is best understood as an analog to satellite collision determination in Earth orbit. The method used to detect possible collisions between two satellites in Earth orbit implements positional uncertainty ellipsoids that surround each satellite in question. Here, the two objects in question are an asteroid and the Earth itself. The analogy diverges, however, when we speak about the two objects influencing one another gravitationally. In Earth orbit, the two satellites do not have a gravitational effect on one another, whereas in the scaled up version, the Earth (one of the objects in the collision) influences the asteroid gravitationally. This is realized in the choice of dynamic model, namely the Restricted Problem of Three Bodies where the Sun and the Earth influence each other and the asteroid, but the asteroid does not reciprocate.

The dynamic model used in this study is relatively simple. Other, more sophisticated models for propagating the orbits of asteroids are being put to practical

use in systems such as the National Air and Space Administration's (NASA's) Horizons[1] software program. The specific model used for dynamic propagation is not tied directly to the method to calculate the probability of collision. Advancing dynamic modeling techniques of asteroids is not intended to be a contribution of this thesis. One may substitute any dynamic model one chooses into the analysis and still benefit from the work done here on the probability calculation.

The contributions of this thesis can be summarized in the following way. This thesis develops an alternative approach to the calculation of collisional probability of asteroids and the Earth. It bases its methods on those used to calculate collisions between Earth orbiting satellites, which use positional uncertainty ellipsoids surrounding each satellite. The development of these methods as applied to asteroid/Earth cases—loosely based on real asteroids—is then followed by an analysis of the effect of variable initial uncertainty on the probability calculated. Understanding this relationship is the second main contribution of this thesis. It is not a contribution of this thesis to develop new techniques of dynamic modeling, or to present results of more accurate probabilities than those produced by current automated systems.

Before these can be addressed, a few introductory points must be established. These include the reason to study asteroid impacts and related work being done in Earth orbiting satellite collision probability determination. The methods currently in place today to calculate asteroid impact probability are also presented briefly. This chapter concludes with a summary of the approach taken in the remaining chapters.

1.1 Motivation

The motivation for such work is apparent. Asteroid impacts are the only natural disaster that can, in theory, be prevented. The first step in preventing such an event from occurring is predicting its occurrence. If a high probability event is detected and confirmed, we can, with present or near-term technology, take steps

---

[1]a telnet and online software program by NASA's Jet Propulsion Laboratory (JPL) that produces the ephemerides of bodies in the solar system such as the planets and asteroids. The output can be customized into several different reference frames and formats [1].

to possibly deflect an object from a collision course. One of the only limitations on our ability to prevent an impact is the amount of lead-time we are given to the event. If a collision is not detected early enough, we may not be able to do anything but wait. Developing techniques for determining the probability of an event is then the second line of defense against a possible asteroid impact (the first being observation of the asteroid). This defense is important because of the consequences of such an event and the likelihood of it occurring at all. A brief look at history sheds some light on these two factors.

1.1.1 Frequency and Consequences of Impact

With the advent of artificial satellites in the mid-twentieth century, we saw, for the first time in human history, our home from outside the atmosphere. It was the beginning of the Cold War and the use of these satellites for reconnaissance was realized quickly. Systems like the Defense Support Program (DSP) were developed to alert the US government of foreign aggressive missile launches. But the program collected data on more than just its intended purpose. The DSP program observed flashes of light in the upper atmosphere that required extensive examination to be differentiated from military activity [2]. What they actually saw were small meteors impacting the atmosphere that were visually undetectable on the ground. In fact, the flashes of light in the upper atmosphere happen on a regular basis as a result of the impact of small, extraterrestrial, non-man-made objects. The objects that cause this type of phenomena are less than 5 m in diameter [3].

Objects about 10 m in diameter impact annually [4]. Depending on their size and velocity, objects of this size can reach near to the surface before vaporizing and cause significant damage to property and vegetation. Larger objects, 50 m in diameter, impact the Earth on average every several hundred years [5]. These cause substantial local destruction but pose no threat to the planet as a whole. Generally speaking, the cut off diameter between a devastating but local event and a global catastrophe is considered to be one kilometer [6] [7].

According to the NASA Ames Research Center [6], objects on the order of a few kilometers in diameter impact on average every hundred thousand years and pose a significant threat to society and possibly life itself. The mass of such an object

is several tens of billions of tons. An impact by such an asteroid would result in a ground burst explosion with energy on the order of a million megatons of TNT. An impact by an asteroid a few kilometers wide would result in global temperatures being depressed by the large amounts of dust thrust into the stratosphere [6]. Agriculture across the globe would be affected and the climate would change significantly. Other effects include acid rain and firestorms from fragmented debris of the asteroid raining down over a large area [5]. If the asteroid hit water, massive tsunamis several kilometers high would reach significantly far inland, which may cause more damage than a similar impact over land [4]. All of this would be a substantial turning point in human history. The capacity of the world's utility, transportation, communication, food source and other infrastructures would be significantly reduced. Life would be altered dramatically for any who survive the initial impact of an asteroid at least a kilometer in diameter.

While these cause significant surface and climatic effects, impacts of this size or larger would not have a significant effect on the celestial properties of the Earth such as angle of tilt, mass, or orbit about the Sun (length of day or year). Only an object of comparable mass to the Earth could cause such effects [8].

All of these are a consequence of ever diminishing probability of impact. Nevertheless, objects of smaller size cause enough damage to justify significant research in the field of Asteroid Detection and Impact Monitoring.

1.1.2 Historical Impacts

A quick glance at the moon on a clear night should be all the evidence required to convince someone that objects collide with the larger bodies of the solar system. While Earth's atmosphere protects it from most of the objects that come close and erodes evidence of past impacts, the shear number of impact craters visible by the naked eye on the Moon shows the frequency of such events.

The time between the 4 and 3.8 billion years ago is sometimes referred to as the late heavy bombardment [9]. As the name suggests, during this time the Earth was bombarded by debris from the early formation of the planets. Also during this time, it was impossible for life to take hold because of the chaotic environment. It is believed that one of the last impacts of this period brought to Earth the

final ingredients for life. Fossil records date surprisingly close to the end of this period [5]. No direct evidence remains of the impacts during this period for two reasons: the individual impacts were clouded by one another and the overall violent nature of the era and, also, Earth's outer crust has been continually folded and recycled by plate movement and volcanic activity over the past 3 billion years, not to mention atmospheric weathering of any smaller craters [10].

The oldest known event to have taken place on Earth happened in Suavjarvi, Russia approximately 2.4 billion years ago. It left a crater approximately 16 km in diameter. A more recently discovered crater in South Africa is the remnant of an impact about 2 billion years ago. This one, referred to as Vredefort, is the largest confirmed impact event since the Hadean and was caused by an asteroid roughly 10 km in diameter [11].

The most well known impact event on Earth occurred near the Yucatan Peninsula 65 million years ago. It it theorized to have caused a mass extinction across the globe, which included the dinosaurs. We humans may be able to thank this event for our dominance of the food chain. The organisms that survived this event were burrowing mammals, who flourished in the mostly predator free environment following the event and from which we are evolved [12].

More recent impact events are not clearly asteroid impacts because no definitive craters exist. In 1908, an explosion over Siberia was witnessed my local herdsmen and destroyed a 50 km wide area of forest. Figure 1.1 shows the resulting destruction. It is suspected to be from an object burning up in the lower atmosphere and referred to as the Tunguska Event. In 2002 an event occurred over the Mediterranean, which was most likely an asteroid burning up in the low atmosphere, but again, no crater exists. While the Mediterranean event caused no significant property damage it posed an indirect threat that has already been mentioned unique to the modern human: explosions in the atmosphere may be mistaken for artillery or nuclear weapons being used, which could erupt into actual conflict [4].

In 2008, the first asteroid to be detected before impact was 2008 TC3. It was spotted by astronomers at the University of Arizona and confirmed by others within hours. Despite the early warning, the predictions for impact were very accurate because astronomers were spread across the globe and could easily compare data. 2008 TC3 burned up in the atmosphere somewhere over the Sudan. Because of the

Figure 1.1. The forest near Tunguska. This photo was taken in 1927 by an expedition to the site. [13]

remote location, very few people witnessed the explosion. Only the crew and some passengers of an airline flight saw a flash of light in the distance at approximately the time predicted [14].

Impact events are not unique to the Earth and the Moon, of course. In 1994, the Shoemaker-Levy 9 comet impacted Jupiter in a spectacular display. It had been captured into an orbit around Jupiter and made a very close approach in 1992 [15]. Because of its mass, Jupiter is more likely to capture a large object than is the Earth, but this event shows that objects of appreciable size do collide with the planets [16].

Impact events large and small have occurred with frequency on the Earth since its formation. Some have caused mass world extinctions and others most likely deposited necessary life materials. The human species has in the past and may in the future be influenced substantially by an impact event. Some believe based on the rates at which objects have struck the Earth in the past, that we are due for a large impact in the coming centuries.

1.2   Related Work

This section discusses work being done in asteroid impact detection and in satellite collision detection. Both fields aim to calculate the probability of collision between two objects.

Automatic asteroid detection systems in use today use a method to calculate probability called the Line of Variations to calculate impact probability. The alternative discussed in this thesis is more closely related to the work being done in satellite collision detection.

1.2.1 Asteroid Impact Detection and the Line of Variations

Asteroids, as a threat, have been studied with fervor for the past 15-20 years. Ever since the comet Shoemaker-Levy 9 collided with Jupiter, interest in a possible Earth impact has spiked [4].

Near Earth Objects (NEOs) are defined as objects with a perihelion distance less than 1.3 Astronomical Units (1 AU is the distance between the Sun and the Earth). They pose a higher threat of impact than objects with a higher perihelion distance. These objects are actively searched for by automated systems.

The search for NEOs has had enormous success in the past 10 years. From 1990 to 2000, there was an increase in known NEOs by a few hundred. Between 2000 and 2010 there was an increase in the number of known NEOs by more than 6000. According to NASA's JPL Near Earth Object website [5], to date (September 9, 2010) there have been 7141 NEO discoveries. The figure was 6994 on January 1, 2010. The majority of objects in this list are between 300 to 1000 meters in diameter.

There are many systems in place around the world that are tasked with tracking these objects and running search algorithms on this catalogue to detect possible impact events. Some of these are [5]:

- the Lincoln Near Earth Asteroid Research (LINEAR) program at the Massachusetts Institute of Technology (MIT)

- the Spacewatch program at the University of Arizona

- the Lowell Observatory Near Earth Object Search (LONEOS)

- the Sentry program at JPL

- the Catalina Sky Survey also at the University of Arizona

- the Japanese Spaceguard Association (JSGA)

- the CLOMON2 program at the University of Pisa

- the Campo Imperator Astronomical Observatory in Italy and

- the Near Earth Asteroid Tracking (NEAT) program at JPL

NASA's automated search algorithm called Sentry in collaboration with the University of Pisa's CLOMON2 system have paved the way in searching for potential impactors among these catalogued entries. They are independent systems; each uses a method for calculating the probability of impact called the Line of Variations (LOV).

The LOV is the string of virtual asteroids (VAs) that are propagated from the confidence region in the six-dimensional configuration space of orbital elements to the target plane (the two-dimensional plane with the Earth cross section at the origin). The question is how to sample the confidence region to obtain a meaningful LOV. Random sampling is possible and makes up Monte Carlo methods. The most efficient LOV sampling occurs when the VAs are uniformly spread along the LOV [17]. Random sampling does not provide proper efficiency, so an analytical definition of the LOV is required.

Several definitions for the LOV can be found in [17] [18] and [19]. Once the LOV is found and propagated to the target plane, probability of impact is calculated by counting the number of VAs that lie within the cross section of the Earth.

This work is ongoing and being pursued at NASA JPL and the University of Pisa, Italy. This thesis is not concerned with this work other than acknowledging that it exists. The field of Earth orbiting satellite to satellite collision detection is a good place to look for an alternative to this approach. The methods used for that purpose can be scaled up and applied to asteroid impact detection.

1.2.2 Satellite Collision Detection in Earth Orbit

With the number of objects in Earth orbit growing rapidly, efforts are made continuously to detect conjunctions between those objects. Usually, one of the objects in question is an active, controllable satellite, so that, in the case of a high probability conjunction, it can be maneuvered to a safe position.

Probabilities are calculated for possible collisions during launch and for high value missions during operation. The method most commonly used for this purpose takes advantage of the positional uncertainty ellipsoids of the active object and the rogue debris (the primary and secondary objects, respectively). The uncertainties of the two objects are combined into a total uncertainty. This total uncertainty is then placed on the center of the primary. The combined radius is the sum of the two effective radii of the objects and is then assigned to the nominal position of the secondary. Probability is calculated by integrating the uncertainty over the volume swept out by the secondary object.

Chan [20, pp. 77-97] makes a distinction as to whether the encounter can be considered short-term or long-term with regards to the time that the objects spend in the encounter region. As a general rule, objects in Low Earth Orbit can be considered short-term, while objects in Geosynchronous Orbit can be considered long-term, but this is not always the case. For short-term encounters, Chan then takes steps to reduce the three-dimensional integral by integrating over the direction of relative velocity. Because the uncertainty is highest in this direction, along with the linear approximation, it can be integrated from negative infinity to positive infinity thus producing unity in this direction. The remaining integral is then easier to handle computationally and subject to the assumption of linearity.

Chan goes on to caution that the two-dimensional integral cannot be obtained by a transformation of the three-dimensional covariance matrix onto the target plane [20, pp. 60], as proposed by Klinkrad in [21]. According to Chan, such a transformation assumes out any possibility of conjunction before or after the target plane, which is not the case for a three-dimensional uncertainty ellipsoid.

This thesis approaches the problem of asteroid impact probability in much the same way as satellite conjunction probability. It presents a method for calculating the impact probability of an asteroid by utilizing the positional uncertainty ellipsoid.

1.3 Approach

The main difference between the approach of this thesis and the method presented in the last section is as follows. First, the primary object (the Earth) gravitationally

influences the secondary (the asteroid). And second, the uncertainty of the primary object is assumed zero: the ephemeris of the Earth is known orders of magnitude more accurately than the asteroid.

The dynamic model employed here is the Restricted Problem of Three Bodies. This takes into account the gravitational influence of the Earth on the asteroid as well as that of the Sun. This problem has no analytical solution [22] so the integration is performed numerically. The solution to the three-body problem is denoted as the nominal solution. It does not represent the actual trajectory of the asteroid. The actual trajectory of the asteroid is unknown.

What is known, however, is the three-dimensional Gaussian probability density function (pdf) surrounding the asteroid at the initial epoch. This pdf is the uncertainty in position represented by an ellipsoid whose surface is 3σ, where σ is one standard deviation. Mathematically, the ellipsoidal pdf is a 3×3 positional covariance matrix and can be propagated forward in time subject to the three-body dynamics—as the asteroid is propagated along its orbit, so too does the uncertainty deform.

The construction of the total probable asteroid solution then comes in two parts. The first part is the nominal solution of the asteroid orbit (based on the initial position and velocity). The second part is the rotation, expansion, and/or compression of the uncertainty ellipsoid as a function of time. The two parts are then connected in the following way: the uncertainty ellipsoid at each time step has as its center the nominal solution at that time. Both the trajectory of the asteroid and the behavior of the uncertainty are results of the three-body dynamics.

Like the nominal trajectory of the asteroid, the behavior of the uncertainty is also subject to initial conditions. This initial uncertainty is one of the main focuses of this thesis. Recall that a relationship between variable initial uncertainty and final probability is desired. This variability can be accomplished in several ways. This thesis uses a Monte Carlo method to randomly select the initial uncertainty from a sampling space. With the initial uncertainty, using the three-body dynamics, the uncertainty at any future time can be determined.

Once the total solution is obtained from the dynamics, the asteroid and the uncertainty ellipsoid are propagated to a region of encounter. This region can be understood at this point simply as a region in space in which the probability of

collision is desired. The probability is then calculated by integrating the three-dimensional Gaussian pdf over the volume swept out by the Earth during the encounter. This last statement is a simplification because the probability ellipsoid is not held constant during the encounter.

This process—from development of the dynamic model to the Monte Carlo simulation and probability calculation—is the focus of the remaining chapters.

1.4 Reader's Guide

- **Chapter 2: Dynamics** discusses two dynamic models. It presents, first, the three-body problem and then the more computationally complex multi-body problem. It then evaluates the benefit of using the three-body problem for this study instead of the multi-body problem, focusing on the trade off between complexity and accuracy. Following this discussion, Chapter 2 includes a description of the numerical methods used to solve the equations of motion.

- **Chapter 3: Uncertainty and the Calculation of Probability** describes sources of uncertainty, how it is represented mathematically, and discusses how the three-body dynamics are used to handled the uncertainty throughout the solution. It then defines the encounter regions and the integrals used to calculate the probability of collision.

- **Chapter 4: Monte Carlo Simulation Results** starts with a description of the Monte Carlo simulation and then presents the results of the implementation of the methods discussed in Chapters 2 and 3 for three hypothetical cases loosely based on the asteroids Apophis, 1999 RQ36, and 2010 RF12. The trends in probability vs. initial uncertainty for each case are then analyzed. The probabilities calculated are not intended to be the latest estimates of impact probability for these asteroids. They are only given as examples of the implementation of the methods discussed.

- **Chapter 5: Conclusions** explains the trends seen in Chapter 4 and summarizes the contributions and limitations of the methods described in Chapters

2 and 3. In light of the limitations, this chapter suggests work in the future that could increase the applicability of these methods to accurate asteroid cases that produce actual probabilities of impact.

Chapter 2

Dynamics

The dynamic model is the foundation of the probability analysis. Without it, no meaningful result can be practically achieved: the analysis would only be mathematical. With it, it can be better understood how the uncertainty affects the probability of impact in a real sense, one that can be applied to real asteroids. The dynamic model is the first step in calculating the probability of impact; it is the roadwork upon which this analysis finds its destination.

The dynamic model is required to produce two results that are used in the calculation. It should give the nominal trajectory of the asteroid and allow for the propagation of the uncertainty ellipsoid. That is, the result of the dynamic model should be the dynamic gravitational (numerical) solution and the state transition matrix. Also, the model should be simple in extent and easy to employ, without adding extraneous points of failure that only hinder the advancement of the analysis overall by inducing unnecessary doubt in the result. This last requirement is specific to this study and can be interpreted, modified or ignored depending on the circumstances of the analysis.

The problem is as follows. An asteroid is free to move in three-dimensional space subject to the gravitational influence of a set of massive bodies under mutual gravitational influence. The nominal trajectory of the asteroid is the primary concern. Two types of models are discussed in this chapter. The first is the Circular Restricted Three Body Problem (CR3BP) consisting of two massive bodies (the Sun and the Earth) on circular orbits. The second is a multi-body problem consisting of eight planets, Pluto, the Moon, and three massive asteroids on in-

clined elliptical orbits. Each model is of a "restricted" nature, that is the mass of the asteroid is assumed to be small enough that it does not contribute any gravitational influence on the other massive bodies.

This chapter covers the process to find the dynamic model that best fits our needs and solves the problem, as stated previously. Specific scripting techniques are discussed for modeling the asteroid in orbit around the Sun subject to other perturbing bodies, including the Earth.

Several models can be employed that provide these requirements. The simplest case is the two-body problem of the asteroid and the Sun, which will not be discussed here. Next in complexity, the Earth is included in the three-body problem. Lastly, the eight planets, Pluto, the three largest asteroids and the Moon are included in what is called the multi-body problem. The equations of motion are presented for these two models and numerical methods to solve them are discussed in Section 2.3.

2.1 Three-body Dynamics

2.1.1 Preliminary Setup

CR3BP is usually formulated in a frame that rotates with the orbits of the primaries, so that they are stationary in the frame. As seen in Figure 2.1, the x-axis is defined as the line connecting the two primaries (the Sun is the primary and the Earth is the secondary body) and points towards the primary. The z-axis is parallel to the angular velocity of the system, and the y-axis completes the right-handed system. The origin is at the center of mass of the system.

The mass unit is the total mass in the system (because the third body is of negligible mass, the total mass is $M_1 + M_2$). The mass ratio of the system, μ, is then the normalized mass of the less massive secondary body. This is an arbitrary choice, m_1 can be suitably chosen as well.

$$m_1 = \frac{M_1}{M_1 + M_2} = 1 - \mu \qquad m_2 = \frac{M_2}{M_1 + M_2} = \mu \qquad (2.1)$$

Normalized masses are lowercase while actual masses are uppercase.
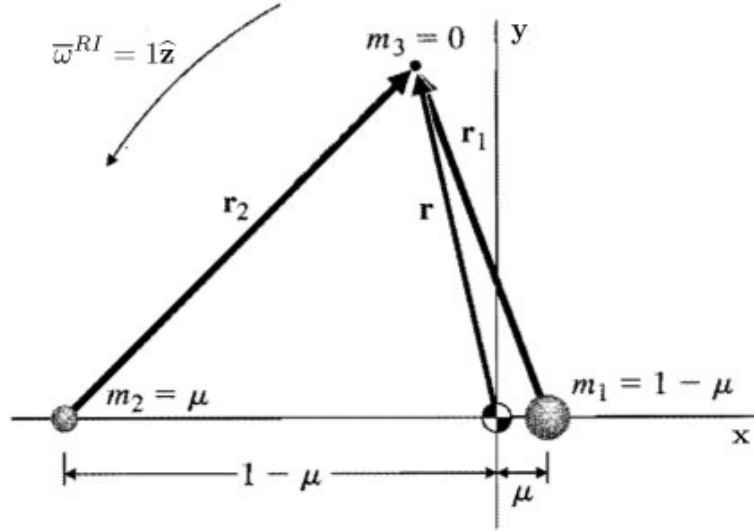
Figure 2.1. Arrangement of the bodies in the rotating frame [22].

The length unit is chosen to be the distance between the primaries, r_{12}. To find the positions of the primaries with respect to the center of mass of the system, multiply each of the masses by their respective distances from the origin and set the sum to zero: $m_1 x_1 + m_2 x_2 = 0$. The distance between the primaries is normalized to one, $r_{12} = x_1 - x_2 = 1$, which gives $x_1 = \mu$ and $x_2 = \mu - 1$.

2.1.2 Equations of Motion

Because the frame of CR3BP is rotating with the primaries, the inertial acceleration of this rotation must be taken into account. The equations of motion are found by equating this inertial acceleration with the gravitational acceleration felt by the third body.

The gravitational accelerations are developed from Newton's inverse square law. First, the radii from each of the primaries to the third body in the [x,y,z] space are defined. The y component of these radii is just the distance from x-axis along the $\hat{y}$ direction. Because each body is on the x-axis, that component is simply y. The same goes for the z component. It is simply z because the primaries are in the x-y plane. The x component, however, must take into account the distance of the two primaries from the origin. Subtracting x_1 and x_2 from x, for r_1 and r_2,

respectively, accomplishes this. The distances to the third body from m_1 and m_2 are:

$$r_1 = \left[(x - \mu)^2 + y^2 + z^2\right]^{\frac{1}{2}} \tag{2.2}$$

$$r_2 = \left[(x + 1 - \mu)^2 + y^2 + z^2\right]^{\frac{1}{2}} \tag{2.3}$$

The gravitational acceleration in the inertial frame (superscript I) felt by the third body as influenced by the two primaries is then,

$$^I\frac{d^2\bar{r}}{dt^2} = -\frac{(1 - \mu)\bar{r}_1}{r_1{}^3} - \frac{\mu\bar{r}_2}{r_2{}^3} \tag{2.4}$$

The inertial acceleration in the rotating frame (superscript R) is given by,

$$^I\frac{d^2\bar{r}}{dt^2} = {}^R\frac{d^2\bar{r}}{dt^2} + 2\bar{\omega}^{RI} \times {}^R\frac{d\bar{r}}{dt} + \bar{\omega}^{RI} \times (\bar{\omega}^{RI} \times \bar{r}) \tag{2.5}$$

where the position, velocity and acceleration of the third body in the rotating frame and $\bar{\omega}^{RI}$ are:

$$\bar{r} = x\hat{x} + y\hat{y} + z\hat{z} \tag{2.6}$$

$$^R\frac{d\bar{r}}{dt} = \dot{x}\hat{x} + \dot{y}\hat{y} + \dot{z}\hat{z} \tag{2.7}$$

$$^R\frac{d^2\bar{r}}{dt^2} = \ddot{x}\hat{x} + \ddot{y}\hat{y} + \ddot{z}\hat{z} \tag{2.8}$$

$$\bar{\omega}^{RI} = 1\hat{z}$$

The dots represent derivatives with respect to time and the hats represent unit vectors in the three mutually perpendicular directions.

The term $\bar{\omega}^{RI}$ is the angular velocity of the rotating frame with respect to the inertial frame. It is unity because of our choice of time unit. The time unit is chosen such that the gravitational constant, G, is one. From Newton's Third Law, because r_{12}, G, and $(m_1 + m_2)$ are all unity, the period of the primaries is just 2π. It follows then that the angular velocity, which is one period per 2π radians, is one.

Evaluating the cross products of equation (2.5) and grouping by component,

$$^I\frac{d^2\bar{r}}{dt^2} = (\ddot{x} - 2\dot{y} - x)\hat{x} + (\ddot{y} + 2\dot{x} - y)\hat{y} + \ddot{z}\hat{z} \tag{2.9}$$

Now equating equations (2.4) and (2.9) and splitting into components the three equations of motion for CR3BP are

$$\ddot{x} = 2\dot{y} + x - \frac{(1-\mu)(x-\mu)}{r_1{}^3} - \frac{\mu(x+1-\mu)}{r_2{}^3}$$

$$\ddot{y} = -2\dot{x} + y - \frac{(1-\mu)y}{r_1{}^3} - \frac{\mu y}{r_2{}^3} \tag{2.10}$$

$$\ddot{z} = -\frac{(1-\mu)z}{r_1{}^3} - \frac{\mu z}{r_2{}^3}$$

These equations are highly non-linear. Many attempts were made in the 100 years following the formulation of the three-body problem to solve it analytically. In 1899, Poincare proved that it was unsolvable in closed form [22].

The numerical solution to these equations is described in Section 2.3 and Appendix A.1.

2.2   The Multi-Body Problem

The multi-body problem[1] is presented here in the inertial frame with the origin at the barycenter of the system. The frame is Horizons' ICRF/J2000 [1] defined with the x-axis pointing out along "the ascending node of the Earth's orbit and the Earth's mean equator [1]", the z-axis perpendicular to the Ecliptic plane at the reference epoch, and the y-axis completing the triad. The problem is essentially an extension of the two-body problem, which is simply Newton's Universal Law of Gravitation in vector form. The equations of motion [23] are:

$$\ddot{\bar{r}} = -\frac{\mu\bar{r}}{r^3} + \sum_{k=1}^{N} \mu_k \left[\frac{\bar{r}_k - \bar{r}}{|\bar{r}_k - \bar{r}|^3} - \frac{\bar{r}_k}{r_k{}^3} \right] \tag{2.11}$$

where $\bar{r}$ is the position vector, μ, in this section only, is the gravitational parameter, the subscript k represents the perturbing body, and N is the number of perturbing bodies. The solution of equations of motion like these is discussed in Appendix A.1. The question that remains to be answered to solve equation (2.11) is how to

---

[1] The definitions of μ and the [x,y,z] frame are suspended for this section and are re-defined. These re-definitions only hold for the multi-body problem. The definitions for these quantities in all other cases can be found in Section 2.1

obtain the positions of the perturbing bodies at each time step. Two methods to find these positions are discussed.

First of all, ephemerides of the planets and the asteroids are available through various sources [1] [24]. The process in that case is to convert the output of those systems into a useable form so that the exercise is really about handling large amounts of data. The ephemerides must be obtained and converted for the time period desired.

2.2.1 Mean Anomaly

The first method to solve for the positions of the perturbing bodies, in this case the planets, is to use two body dynamics about the barycenter of the solar system. This assumes that the perturbing bodies are on inclined, eccentric orbits. The initial conditions are in the form of the classical orbital elements.

The classical elements can be converted to a three-dimensional position vector. This is done, first, by solving for the radius using the two-body equation of semi-major axis, a, eccentricity, e, and true anomaly, θ:

$$r = \frac{a(1 - e^2)}{1 + e \cos \theta} \tag{2.12}$$

then by rotating a vector of length r initially aligned with the inertial x-axis through three rotations in right ascension of the ascending node, Ω, inclination, i, and the sum of argument of perifocus and true anomaly, $(\omega + \theta)$,

$$\bar{r} = \begin{bmatrix} \cos \Omega & -\sin \Omega & 0 \\ \sin \Omega & \cos \Omega & 0 \\ 0 & 0 & 1 \end{bmatrix} \begin{bmatrix} 1 & 0 & 0 \\ 0 & \cos i & -\sin i \\ 0 & \sin i & \cos i \end{bmatrix} \dots$$

$$\begin{bmatrix} \cos(\omega + \theta) & -\sin(\omega + \theta) & 0 \\ \sin(\omega + \theta) & \cos(\omega + \theta) & 0 \\ 0 & 0 & 1 \end{bmatrix} \begin{bmatrix} r \\ 0 \\ 0 \end{bmatrix} \tag{2.13}$$

where the three 3×3 matrices are direction cosine matrices that make up a single 3-1-3 rotation.

The next step is to advance the true anomaly forward through time. Since true anomaly is not an explicit function of time, this requires several steps. First, calculate mean anomaly, M, which is a function of time:

$$M = \sqrt{\frac{\mu}{a^3}} t + M_0 \tag{2.14}$$

Then, solve for eccentric anomaly by:

$$g(E) = E - e \sin E - M = 0 \tag{2.15}$$

Since this equation is transcendental, it must be solved iteratively to convergence,

$$\dot{g}(E) = 1 - e \cos E \tag{2.16}$$

$$E_{k+1} = E_k - \frac{g(E_k)}{\dot{g}(E_k)} \tag{2.17}$$

(A good first guess for E_k is M). Finally, convert eccentric anomaly to true anomaly by:

$$\tan\left(\frac{\theta}{2}\right) = \sqrt{\frac{1+e}{1-e}} \tan\left(\frac{E}{2}\right) \tag{2.18}$$

With the new true anomaly, the radius vector is rotated into position at the new time step. In this way, the perturbing bodies are advanced forward in their orbits with the rest of the integration.

2.2.2 Propagation

The second way to obtain the positions of the perturbing bodies is to integrate their equations of motion [25], which are:

$$\ddot{\bar{r}}_k = \sum_{j \neq k} \frac{\mu_j (\bar{r}_j - \bar{r}_k)}{|\bar{r}_j - \bar{r}_k|^3} \tag{2.19}$$

where the subscript j refers to another perturbing body.

These equations are evaluated simultaneously for each perturbing body, k, at each time step in the integration of the equations of motion of the asteroid itself. More details are found in Appendix A.2.

2.2.3 Accuracy

Following these methods through coding and simulation results in the position of the asteroid at each time step. This is done for the asteroid 99942 Apophis (previously known as 2004 MN4). The result of these methods is compared to the ephemerides provided by Horizons, which are sufficient to be called the true nominal trajectory.

The result is similar to the Horizons data in its gross characteristics. The orbits of both methods fill a common physical space as seen in Figure 2.2, which also compares the orbit of the Earth. At a glance, they seem comparable. Closer inspection, however, reveals that the orbit paths are not coincident. Furthermore, Apophis and the Earth are not in the same location on their orbits as in Horizons, which is not conveyed in the figure. The error is mostly in-track and can be greater than a full orbit over the 30-year time span. It seems as though the problem is very sensitive to the magnitude of the initial velocity because the two models predict different average speeds of the asteroids on their orbits, which is why the error is in-track.

2.2.4 Summary

The procedure laid out in this section for obtaining the nominal solution of the asteroid: integrating the positions of the perturbing bodies at each time step in the integration of the equations of motion, is rather complex. Given that this method does not produce the accuracy desired, it is clear that there are unknown variables that state-of-the-art ephemerid programs, like Horizons, take into account. For instance, the methods described here do not take general relativity into account, which Horizons does. Accomplishing the task of replicating perfectly the work of Horizons requires the Horizons team and resources and is outside the scope of this study.
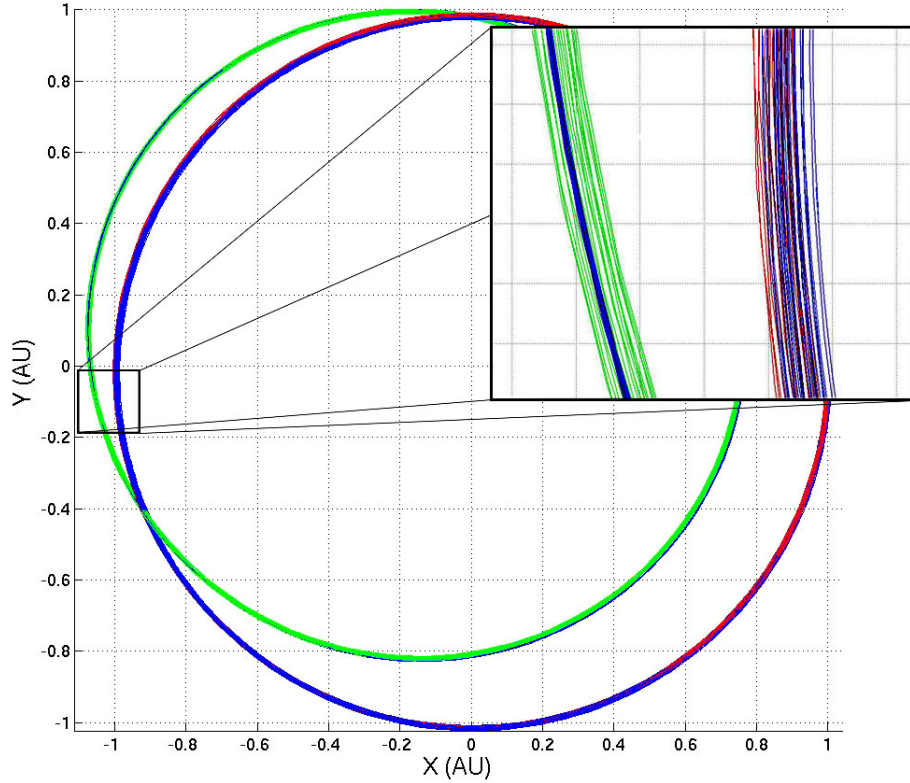
Figure 2.2. Comparison of the methods described in the text for the multi-body problem (blue orbits) with Horizons (green orbit for Apophis and red orbit for the Earth) over a 30-year integration. The reference frame is ICRF/J2000 and is described at the beginning of Section 2.2.

The dynamics used from now on are for simplicity and do not claim to be accurate. They are simply a stand in for a more sophisticated dynamic model that can be done in the future.

For its simplicity and quick run time, the Circular Restricted Three-Body Problem works adequately to fulfill the needs of this thesis.

2.3 Numerical Methods

The backbone of any dynamic model is the equations of motion. They embody the mechanics of the problem in a simple, efficient manner. In almost all cases in orbital mechanics, the equations of motion cannot be solved analytically and exactly. In recent decades this has not posed a significant problem with the use

of computationally numeric methods. Today, the numerical integration of the Newtonian equations of motion for orbital dynamic propagation is well understood. More details are found in Appendix A.1.

The equations of motion for Newtonian gravitation are non-linear, second-order, differential equations. The solvers can handle non-linearity with ease, but the second-order equations require a reduction in order to be used. This is accomplished by defining a state vector of the three-dimensional position and velocity (six equations in all). Defining the state vector as the position and its derivative allows the second order equations to be hidden in a first-order vector differential equation that can be handled by the solver. Now, the relation between position and velocity is explicitly stated by writing the first three differential equations as: the derivative of the first three states is the last three states.

$$
X = \begin{bmatrix} x \\ y \\ z \\ \dot{x} \\ \dot{y} \\ \dot{z} \end{bmatrix} = \begin{bmatrix} x(1) \\ x(2) \\ x(3) \\ x(4) \\ x(5) \\ x(6) \end{bmatrix}
\tag{2.20}
$$

$$
\dot{X} = \begin{bmatrix} \dot{x} \\ \dot{y} \\ \dot{z} \\ \ddot{x} \\ \ddot{y} \\ \ddot{z} \end{bmatrix} = \begin{bmatrix} x(4) \\ x(5) \\ x(6) \\ F_4(X) \\ F_5(X) \\ F_6(X) \end{bmatrix}
\tag{2.21}
$$

But it is already stated that the first three states are the position and the last three states are the velocity. This seems trivial, but it is actually quite subtle. The first order differential equation that is written in vector form is not inherently required to reflect the physics. It could be defined arbitrarily. The solver is a machine that calculates regardless of the physics. It is the programmer who applies the principles of physics. He or she takes advantage of the relation between position and velocity to create a loophole in the solvers functionality. The solver is only

aware of the loop by the explicit definition of one state to the other, which is the correct relation for position and velocity.

Notice, now, that the second order equations of motion are in $F_{4,5,6}$. However, as far as the computer is concerned it is solving a first order vector differential equation. This is what is meant by reduction of order.

2.4   State Transition Matrix

Solving the three-body problem is only half the problem. It gives only the nominal solution, it does not take into account the uncertainty. To do this, the State Transition Matrix (STM) must be found. The STM is used to propagate the initial uncertainty to any future time. The nominal solution gives the trajectory of the center of the uncertainty ellipsoid, while the STM gives the change in orientation and shape of the ellipsoid, based on the dynamics of the three-body problem. The STM is developed from the linearization of the equations of motion. At each time step in the integration, a 6×6 matrix of partials of the equations of motion is calculated and is used as the proportionality constant relating the STM to its derivative [26].

$$\frac{d\Phi(t, t_0)}{dt} = A(t)\Phi(t, t_0) \tag{2.22}$$

$$\Phi(t_0, t_0) = I$$

The STM, Φ, is time dependent and n×n in size, where n is the number of states. The initial STM is the identity matrix. The 6×6 matrix A is the linearization of the equations of motion, F. That is, A is the matrix of partial derivatives of $\dot{X} = F(X)$ with respect to each of the states; it is also called the Jacobian of F.

$$A(t) = \frac{\partial F}{\partial X} = \begin{bmatrix} 0 & 0 & 0 & 1 & 0 & 0 \\ 0 & 0 & 0 & 0 & 1 & 0 \\ 0 & 0 & 0 & 0 & 0 & 1 \\ F_{4,x} & F_{4,y} & F_{4,z} & 0 & 2 & 0 \\ F_{5,x} & F_{5,y} & F_{5,z} & -2 & 0 & 0 \\ F_{6,x} & F_{6,y} & F_{6,z} & 0 & 0 & 0 \end{bmatrix} \tag{2.23}$$

$$
F_{4,x} = 1 + \frac{3(1-\mu)(x-\mu)^2}{r_1{}^5} - \frac{(1-\mu)}{r_1{}^3} + \frac{3\mu(x+1-\mu)^2}{r_2{}^5} - \frac{\mu}{r_2{}^3} \tag{2.24}
$$

$$
F_{4,y} = F_{5,x} = \frac{3(1-\mu)(x-\mu)y}{r_1{}^5} + \frac{3\mu(x+1-\mu)y}{r_2{}^5} \tag{2.25}
$$

$$
F_{4,z} = F_{6,x} = \frac{3(1-\mu)(x-\mu)z}{r_1{}^5} + \frac{3\mu(x+1-\mu)z}{r_2{}^5} \tag{2.26}
$$

$$
F_{5,y} = 1 + \frac{3(1-\mu)y^2}{r_1{}^5} - \frac{(1-\mu)}{r_1{}^3} + \frac{3\mu y^2}{r_2{}^5} - \frac{\mu}{r_2{}^3} \tag{2.27}
$$

$$
F_{5,z} = F_{6,y} = \frac{3(1-\mu)yz}{r_1{}^5} + \frac{3\mu yz}{r_2{}^5} \tag{2.28}
$$

$$
F_{6,z} = \frac{3(1-\mu)z^2}{r_1{}^5} - \frac{(1-\mu)}{r_1{}^3} + \frac{3\mu z^2}{r_2{}^5} - \frac{\mu}{r_2{}^3} \tag{2.29}
$$

The six equations of the pure dynamics are appended by equation (2.22), element by element (36 in total). The resulting set of 42 equations is then solved simultaneously. The solution is linearized at each time step along the solution of the dynamics and the state transition matrix at that time is calculated. The time history of the STM is then accumulated from these individual time steps. Now, the size, shape and position of the uncertainty ellipsoid can be propagated forward in time as dictated by the dynamics of the three-body problem.

Chapter 3

Uncertainty and the Calculation of Probability

Uncertainty is the primary contributor to the "probability" of collision. It stems from observational techniques and initial orbit determination and persists for the reasons discussed in this chapter.

3.1 Uncertainty

Uncertainty in the position of the asteroid comes from two primary sources. The first is that the observational techniques used (telescopes and radar) are limited in their accuracy and subject to random noise. This uncertainty can be accounted for by understanding the equipment being employed. The second source of uncertainty is the limited number of observations possible to compute the orbit. Achievement of an exact orbit requires observations (assuming perfect observational precision) for all time in the life of the asteroid. Obviously, this is impossible in practice. With only a finite number of observations available, multiple orbits can be fit. These multiple solutions are a range of orbital elements and, therefore, a range of possible positions of the asteroid. This is what is meant by uncertainty—a range of possible positions.

In the absence of observational data or observing equipment, this study, instead, looks at several different values for uncertainty to understand how its variation

affects the final calculated probability. It does this by way of a Monte Carlo simulation.

However the uncertainty is obtained, it must be handled, or propagated, over the course of the solution so that it is available for the calculation of probability when desired. It is necessary to propagate the uncertainty because it is not a constant over the life of the asteroid. An initial uncertainty will change, specifically grow, in the future of any dynamic model for several reasons: first of all, the methods to solve the equations of motion are numerical, so the solution is a mathematical approximation. Most importantly, even if the equations of motion could be solved exactly, they are themselves only an approximation to reality. Additionally, the numerical methods are prone to computational round-off and truncation errors. Also, the orbit of the asteroid is subject to several perturbations not all of which can possibly be taken into account. Even if they are all accounted for, they are approximated by simplified models [27, pp. 1-3].

These unknown and non-exact contributors to the path of the asteroid, numerical and observational uncertainties, are all included in the solution, instead, by dynamic propagation of the uncertainty.

3.1.1 Covariance Matrix

In order to handle the positional uncertainty, it must be described mathematically. This representation is the 3×3 positional covariance matrix. It can be defined several different ways. In this thesis, it will be defined using eigenvalues and eigenvectors.

The covariance matrix is built up from information about the uncertainty ellipsoid, which encloses the physical space in which the asteroid can probabilistically be found. To relate the covariance matrix to the uncertainty ellipsoid, start with the lengths of the principal semi-major axes of the ellipsoid, which are three standard deviations, or 3σ. For simplicity, the 3σ principal axes will be referred to as σ_i. The square of these lengths are defined as the eigenvalues of the covariance matrix. Next, the orientation of the ellipsoid, or the directions of the principal axes, are defined as the eigenvectors of the covariance matrix. By placing the eigenvalues in a diagonal matrix E, and the eigenvectors as columns in the matrix V (making

sure to keep the corresponding eigenvalues and eigenvectors in the same columns of each), the 3σ covariance matrix, P, is then,

$$P = VEV^{-1} \tag{3.1}$$

Because V is orthogonal, P is symmetric.

The diagonal terms of P are the variances in the x,y,and z directions multiplied by 3^2. The off-diagonal terms are the covariances between x-y, x-z, and y-z, which are the 3σ's of each direction multiplied by a correlation coefficient (e.g. ρ_{xy}) which indicates how dependent the uncertainties in the respective directions are. Decomposing the covariance matrix in this way does not directly indicate the orientation of the uncertainty nor does it reveal direct information about the size of the uncertainty ellipsoid (that is, the lengths of the principal axes), so this description will not be used. The eigenvalues and eigenvectors, which describe the uncertainty in the principal directions (orientation and size), is much more revealing.

The uncertainty propagation discussed above is carried out by using the State Transition Matrix. The uncertainty is propagated to any future time by a linear transformation of the STM on the covariance matrix. Details are shown in Appendix B.

Future times for which the uncertainty is desired are called encounters. During encounters, the probability of impact is appreciable and can be calculated. A definition of the region of encounter is required before the calculation can be performed.

3.2   Encounter Region

The probability of impact is not required at every location along the orbit of the asteroid, it is negligible over the majority of it. A definition of a region of conjunction is desired the requirements of which are fulfilled only a small finite number of times. This region of conjunction is called the encounter region. There is no unique way to define the encounter region, but, of course, some ways are more suitable than others. The next two sections discuss one possibility. Section 3.2.3 discusses a better approach.

3.2.1 Close Approach

The encounter region can be defined about a point of close approach. That is, if the asteroid comes within a certain distance of the Earth, the probability of impact can be calculated. This method is the most intuitive: the closer the asteroid is to the Earth, the higher the chance that its impact probability is appreciable. (This is incorrect, but this method is developed further before it is abandoned.)

It is not sufficient to calculate the probability only at the point of close approach. An extended region is required. Recall that the domain of integration is the volume swept out by the Earth through the encounter region. The region surrounding the point of close approach that can be approximated linearly is the extent that is required of the encounter region.

3.2.2 Linear Approximation

The region of the orbit around a reference point that can be considered a straight line is a function of the instantaneous radius of curvature at the point of reference. From the mathematics of parameterized curves in three-dimensional space (which the nominal solution of the asteroid is), the radius of curvature is the inverse of the curvature, κ, given by:

$$\kappa = \frac{|\dot{r} \times \ddot{r}|}{|\dot{r}|^3} \tag{3.2}$$

With the radius of curvature, $R = \frac{1}{\kappa}$, and the angle γ, the length of the tangent is,

$$T = R \tan \gamma \tag{3.3}$$

as seen in Figure 3.1. The maximum γ for which the approximation of the arc, C, by the tangent, T, is valid is 0.1 rad (5.8 deg) (see Appendix C). Doubling T gives the region of linearity.

3.2.3 Ellipsoid

While this approach does give a definite region of conjunction, it does not highlight the most probable impact scenarios. Proximity to the Earth with the possibility of being outside the uncertainty ellipsoid does not mean a more probable collision. In
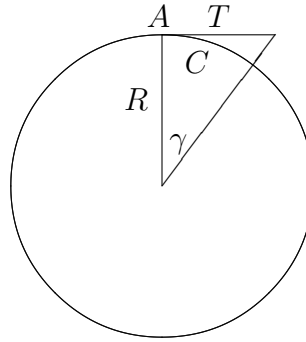
Figure 3.1. The instantaneous circle tangent to the orbit of the asteroid. R is the radius of curvature, the inverse of curvature. T is the linear approximation of the orbit at the point of closest approach, A.

fact, the purpose of the uncertainty ellipsoid is precisely to give a probable location for the asteroid, so it is a better place to look for the definition for the encounter regions.

The encounter region is then defined by saying, if the Earth passes through the uncertainty ellipsoid, then a probability of collision is calculated. By requiring that the Earth be enclosed by the uncertainty ellipsoid, it is guaranteed that the probability calculated is higher than in the first case. If the nominal solution is closer to the Earth but outside the 3σ uncertainty then the probability calculated is necessarily lower than if it were enclosed by the ellipsoid (even if it is radially further away).

This method is non-trivial. The uncertainty along the orbit is not known a priori and cannot be guessed, so that these regions are not regularly spaced along the orbit. The encounter regions depend completely on the dynamics of the system. It may be guessed that the largest semi-major axis of the uncertainty ellipsoid (or the weak direction) is aligned with the velocity vector (that the most uncertainty is in-track[1]), but this does not help to find the encounter regions for two reasons. First, this is not certain. The orientation of the weak direction of the uncertainty

---

[1]A check is made at each time step whether the weak direction of the propagated uncertainty ellipsoid is or is not aligned with the local velocity vector. This check only alerted for the first few time steps, which is expected because the uncertainty is initially aligned with the velocity vector.

ellipsoid does not always align itself with the local velocity vector; there is nothing in the dynamics that requires this. Second, the encounter regions do not occur at locations along the orbit when the velocity vector is pointed towards the Earth.

The initial uncertainty ellipsoid used for Figure 3.2 is aligned with the initial velocity vector, but the values do not correspond to real uncertainty, it is just an example. It is clear from the figure that encounter regions do not retain any pattern.

The method to find the encounter region by checking whether the Earth is inside the ellipsoid (see Appendix D) is advantageous for another reason in addition to
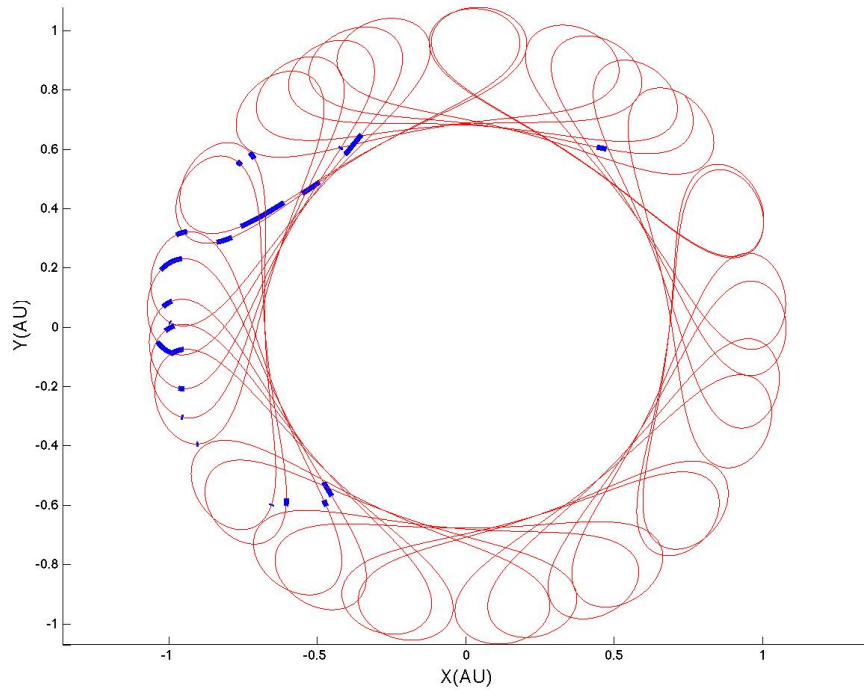
Figure 3.2. This is an orbit based on Apophis in the rotating frame of CR3BP over 30 years (CR3BP is a simplified dynamic model and, therefore, this is not the true nominal trajectory of Apophis). The frame of CR3BP is described in Section 2.1.1. The rotating frame causes the orbit to be shaped as a series of loops that advance in a circle. The Sun is near the origin and the Earth is near (-1,0). This figure also presents the encounter regions (in blue). The uncertainty used for these encounters is arbitrary, the important point is how the uncertainty is oriented and shaped by the dynamics. Note that the encounter regions retain no pattern such as occurring whenever the local velocity vector is pointed towards the Earth.

the one stated above. In the first method for finding the encounter region, the close approach must be checked first, then the region of linearity must be found. The second method gives what is needed to perform a probability calculation in one step.

3.3   Probability Calculation

To summarize what has been done so far: the nominal solution of the asteroid orbit has been found according to the three-body problem; the state transition matrix has been found, which allows for the calculation of the uncertainty ellipsoid at future times; the encounter region has been defined, which is subject to both the nominal solution and the orientation of the uncertainty ellipsoid, which are both in turn subject to the three-body dynamics.

Recall that the uncertainty ellipsoid represents a three-dimensional probability density function, pdf. More specifically, the pdf, f, is a function of the covariance matrix, P,

$$f(x,y,z) = \sqrt{\frac{9}{(2\pi)^3|P|}} \exp\left[-\frac{9}{2} \begin{bmatrix} x & y & z \end{bmatrix} P^{-1} \begin{bmatrix} x \\ y \\ z \end{bmatrix}\right] \qquad (3.4)$$

P^{-1} is the inverse of the 3σ covariance matrix, so it must be multiplied by 3^2 to convert it to 1σ which is how the pdf is defined.

For the probability, this pdf is integrated [20, pp. 47].

$$\iiint_V f(x,y,z)\,\mathrm{d}x\,\mathrm{d}y\,\mathrm{d}z \qquad (3.5)$$

The volume over which this integral is evaluated is the sphere of the Earth, or, for ease of calculation, a cube of equal volume.[2]

Once the probabilities of impact at each time step are calculated according to equation (3.5), they must be combined into a total probability for the encounter. What is being considered are the probabilities of n events (the asteroid impacts at time A or time B), where n is the number of time steps. "Or" is the operative word here. The asteroid can only impact once while it is in the encounter region. All impact events throughout the encounter are mutually exclusive.

According to probability theory, to find the probability of a number of events that are mutually exclusive the probabilities of the events should be added. However, the total probability cannot depend on the number of time steps. If addition is used, increasing the resolution of the dynamic model produces a vastly differing total probability. Also, with enough time steps, it would be easy to see a situation in which the total probability, as a result of simple addition, could be greater than one.

What is needed is a method to accumulate and account for each probability in a way that is independent of the number of time steps. An integration over time accomplishes this. Trapezoidal integration is sufficient for the purposes here. All that is necessary is an order of magnitude. To maintain the order of magnitude of the instantaneous probabilities, the integral is divided by the time span of the encounter.

With the method to calculate probability, it is now possible to examine specific asteroid cases. These are based on real asteroids, but for several reasons that are discussed in Chapter 4, they are not actual cases. It is made abundantly clear that the probabilities calculated for each case are not intended to be taken as estimates of the actual probability of impact. They are just examples. NASA's Horizons program provides the initial conditions of the nominal position and velocity for each case, which are the only parts of the case that are true to reality. The uncertainty data is varied according to a Monte Carlo method so that the relationship between initial uncertainty and resulting impact probability can be examined.

---

[2]The difference in the integral over the two volumes, sphere and cube, is less than 1%, but integrating over a cube is far less computationally intensive and more reliable. The probability is anyway only an order of magnitude, so an error of 1% is acceptable.

Chapter 4

Monte Carlo Simulation Results

This chapter discusses the Monte Carlo method used to obtain the initial uncertainty and presents the results of the simulations for several hypothetical asteroids. The first case is a completely fictitious asteroid on a direct collision course with the Earth. This case establishes the main features of each case based on real asteroids. Finally, the results are summarized.

4.1 Method

Monte Carlo simulations refer to a number of different techniques to obtain a range of data by making random samples. What is being sampled is the covariance matrix, but it is not desired to completely rely on randomized values for each element individually. This would not produce meaningful results because they would not be comparable. The scope of the use of random values must be limited if insightful results are to be obtained. In other words, some feature of the covariance matrix and uncertainty ellipsoid must be held constant over all of the simulations.

It is desired to understand how the amount of uncertainty affects the total probability. So the values for the size of the ellipsoid are randomized while the values for the orientation are held constant.[1]

---

[1] If the orientation is turned to favor the normal direction rather than the in-track direction, as discussed below, the overall trends discussed in this chapter are present, but the specific color trend is different. Results of this type are not presented.

A further limitation on the randomized nature of the simulations is the relative magnitudes of the values being varied. The values that are sampled randomly are the lengths of the principal semi-major axes, σ_i, of the initial uncertainty ellipsoid. The relative magnitudes of these values are (in decreasing order): in-track standard deviation, σ_1, normal, σ_2, and out-of-plane, σ_3. This relationship is imposed in the simulations by defining the range of possible values from which these quantities are sampled.

For these three quantities, four values are required to define the non-overlapping ranges of each. These values are a_k. With a devisor, e, the four values are given by the sequence:

$$a_{k+1} = \frac{a_k}{e} \qquad k = 1, 2, 3 \tag{4.1}$$

where the values a_1 and e are referred to as range values. The ranges are then

$$
\begin{aligned}
a_2 < \quad \sigma_1 \quad < a_1 \\
a_3 < \quad \sigma_2 \quad < a_2 \\
a_4 < \quad \sigma_3 \quad < a_3
\end{aligned}
\tag{4.2}
$$

A uniform random sample is then taken from the range for each value σ.

The procedure is repeated for three different asteroid cases, and 100 times for each asteroid so that a trend in the relationship between initial uncertainty and total probability can be revealed.

4.2   Asteroid Cases

Three asteroid cases are discussed in this chapter. They are based on the real asteroids Apophis, 1999 RQ36, and 2010 RF12. However, the cases are not to be taken as analysis of the real asteroids and their probability of impact with the Earth. The dynamic model is simplified and does not produce an accurate nominal solution. Also, the uncertainty used for each case is unrealistic. These cases share one thing with their real counterparts: the nominal position and velocity at the initial epoch. These were retrieved from NASA's Horizons program [1]. The cases are based on real asteroids for reliability of the cases' long term orbit. It is

possible to consider completely arbitrary cases, but the process of determining a stable orbit over a long time period in CR3BP is a complex issue. By using real initial conditions, the orbits are stable, albeit a deviation from the actual nominal trajectory taken by the asteroid.

Each of the real asteroids is interesting for reasons that will be discussed. Two are Potentially Hazardous Asteroids (PHAs), which are NEOs with a Minimum Orbit Intersection Distance (MOID) of less than 0.05 AU and an Absolute Magnitude (H) of 22.0 or less. MOID is a measure of how close the orbit of the Earth and the asteroid are to one another, a smaller MOID increases the chance that the two will collide if they are in the same place at the same time. Absolute Magnitude can be used to estimate the diameter of the asteroid, a smaller absolute magnitude translates to a larger asteroid. Asteroids that can come close to the Earth and are sufficiently large are PHA's. 2010 RF12 is not a PHA only because it is not large enough. Asteroids that are considered to be of especially high risk are studied individually with great effort by NASA and the University of Pisa, Italy as described in Section 1.2.1.

This chapter presents the results of the algorithm described throughout this thesis as applied to three cases, which are based on the three real asteroids. It offers, for each case, the following:

- The orbit of the asteroid.

- An example of the encounter regions. The encounter regions are dependent mostly on the dynamics and little on the specific values of initial uncertainty (for a given order of magnitude).

- The total probability calculated for each encounter. Two plots will be used to present the relative probabilities. The first plot shows all the encounters over all the runs and uses color for three dimensions and is discussed below. The encounters across each run of the simulation are taken equally. The total probability is plotted against a date associated with each encounter regardless of which of the 100 runs from which it originated. The second plot is a two- or three-dimensional gray-scale plot for single encounters. The second type of plot helps reveal the trend on an encounter-by-encounter basis.

- A list of encounters and their frequency in the 100 runs of the Monte Carlo simulation. This goes to show that the encounters are essentially independent of the initial uncertainty.

For the first type of plot, each data point represents one probability in five-dimensions: the time of the encounter, the value of the probability, and the lengths of the three principal axes of the initial uncertainty ellipsoid. The color of the dot for each probability is defined by a 1×3 vector of numbers between 0 and 1, where each number corresponds to the color red, green, and blue; this scheme is called RGB color. The RGB color space is seen in Figure 4.1. The three values that specify the color are normalized from the lengths of the principal axes. Red, green, blue corresponds to in-track, normal, and out-of-plane, respectively. A black dot signifies that the three principal axes are at the lowest in their respective ranges, and a gray dot signifies they are highest. The background color is outside the range of the normalization so that all probabilities are visible (this is why the highest are gray and not white).
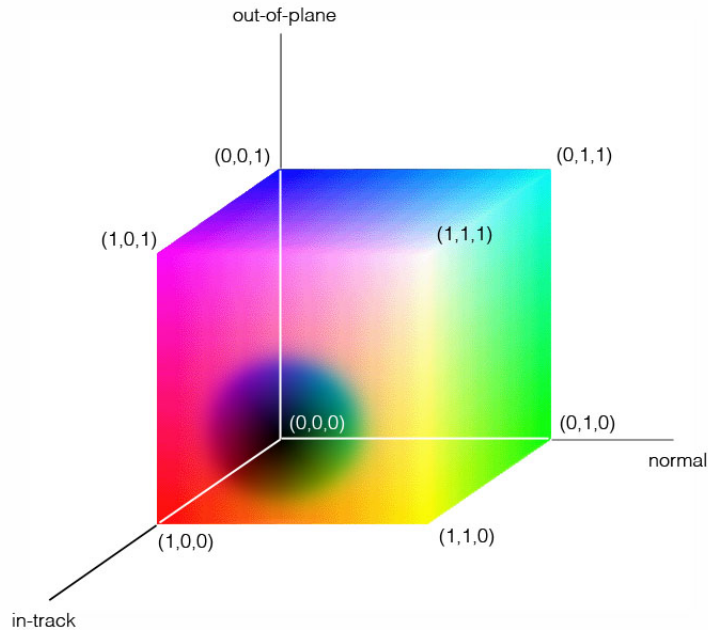
Figure 4.1. The RGB color space is an opaque cube. The origin is seen through a hole in the cube. This figure acts as a legend for the first type of plot which are full page figures displaying total probabilities: Figures 4.3, 4.5, 4.9 and 4.14.

For the second type of plot, the dots for the probabilities are plotted in a three-dimensional space of in-track, normal, and out-of-plane, where the gray scale of the dot represents the relative magnitude of the probability. Dark probabilities are higher and light probabilities are lower.

Note that the convention is opposite for large/high and tight/low for the two plots: larger uncertainties and lower probabilities are both gray dots, while tighter uncertainties and higher probabilities are both black dots. This is done because a darker dot more intuitively corresponds to higher probability (for the second type of plot), but in the RGB color scheme [1 1 1] is very light (in the first type of plot). It is also done to emphasize the different value being conveyed by the shade of the dot in each type of plot.

4.3   Impact Example

Before the three cases are discussed, an example is given for a fictitious asteroid on a direct collision course with the Earth. For this example of an impact scenario, the fictitious asteroid is propagated for 2 days. The short time span is to ensure that the nominal solution does pass through the Earth and also because a longer time span would not be any more revealing. The range values for the initial uncertainty are chosen to be $a_1 = 10^{-4}$ AU and $e = 2$. These values are significantly lower than for the "real" asteroid cases that will follow. This is done because the nominal solution passes so close to the Earth (actually through it) and the initial epoch is so close to the encounter region.

Figure 4.2 depicts several things. First of all, it shows the nominal solution of the fictitious asteroid: the thin red line. Second, it shows the principal axes of the uncertainty (weak: blue, intermediate: green, and shortest: black) superimposed onto several time steps surrounding the encounter (the wide red swath through the Earth). This figure serves two purposes: it shows how high probabilities are achieved by tight uncertainties (relative to the size of the Earth) in close proximity to the Earth during the encounter; it also shows that the uncertainty, for the most part, stays aligned with the local velocity vector but that the weak direction does not. Near the initial condition, in the lower portion of the figure, the uncertainty is coincident with the local velocity vector and stays aligned as such through the
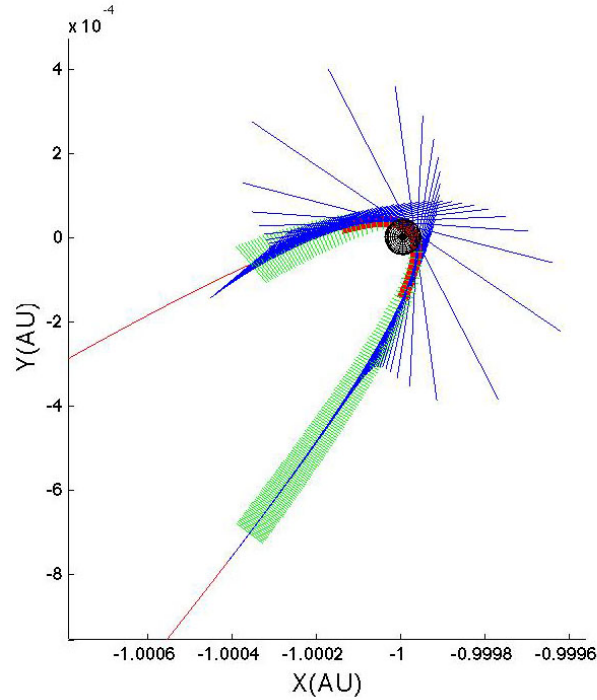
Figure 4.2. A fictitious asteroid on a collision course with Earth. This figure shows the principal axes of the uncertainty at several time steps surrounding the encounter (wide red swath) superimposed onto the nominal solution (thin red line). The weak direction is blue, the intermediate length is green and the shortest is black (for the most part, the black uncertainty is in the unseen out-of-plane direction). Early in time (lower portion), the weak direction is aligned with the velocity vector. As it is propagated through the encounter, the uncertainty remains aligned with the local velocity and does not begin to deviate until after the nominal solution has passed through the Earth.

encounter. After the encounter, the uncertainty starts to deviate from the velocity vector. In general, the uncertainty is aligned with the velocity vector at the start and at a certain point begins to deviate. That point in this case comes after the encounter.

The first type of plot presented for probability is Figure 4.3. The first thing to notice is that the probabilities are not near 100%, even when the asteroid's nominal solution actually passes through the Earth. The reason it is that, first of all, the Earth is finite in extent, so 100% is not possible. Also, the 3σ uncertainty at the time of the encounter is much larger than the Earth. However, despite the low absolute probability, these values are orders of magnitude larger than for the following three asteroid cases, none of which passes through the Earth.
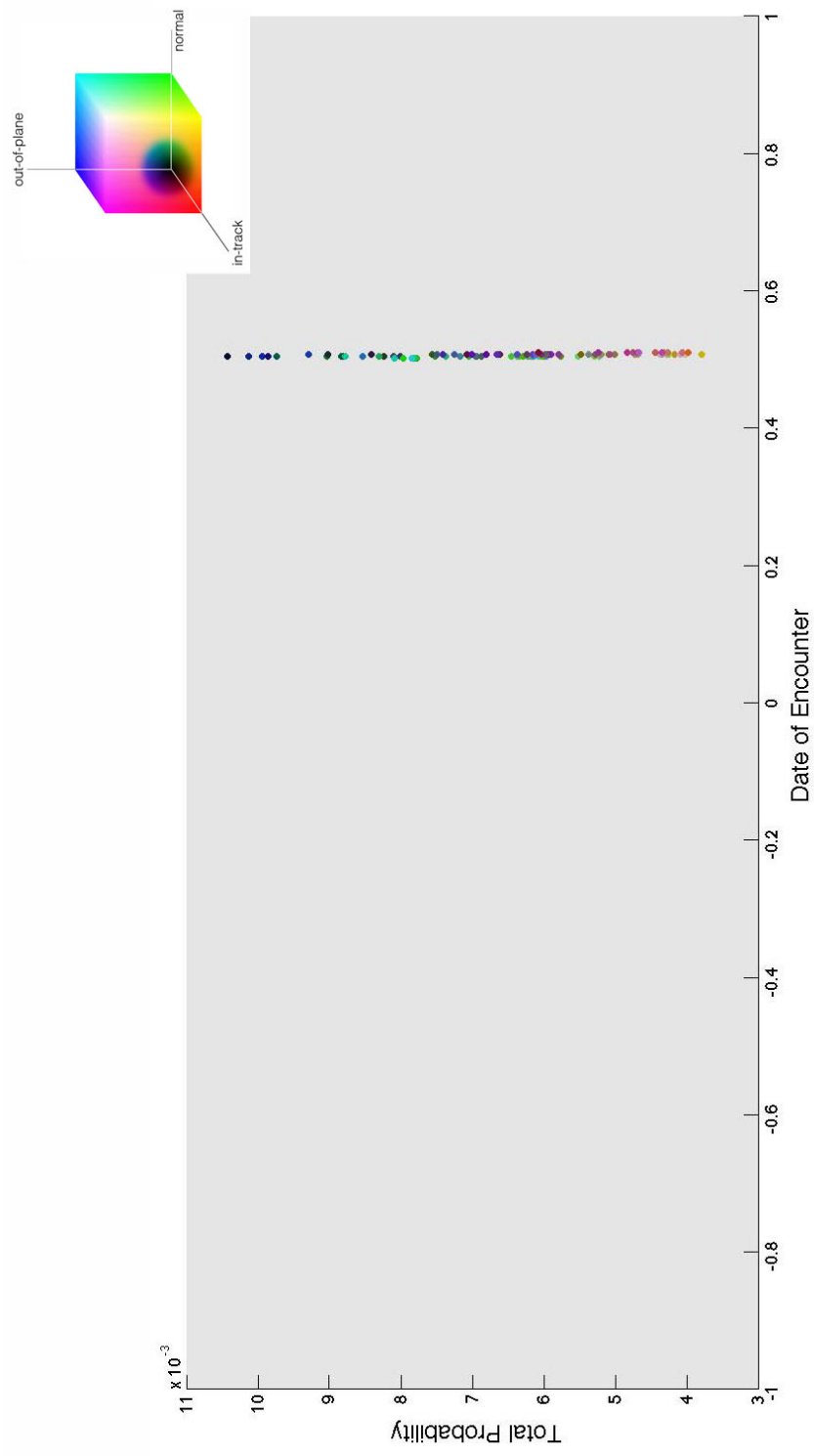
Figure 4.3. The total probabilities of collision with a fictitious asteroid. There is only one encounter when the nominal solution passes through the Earth.
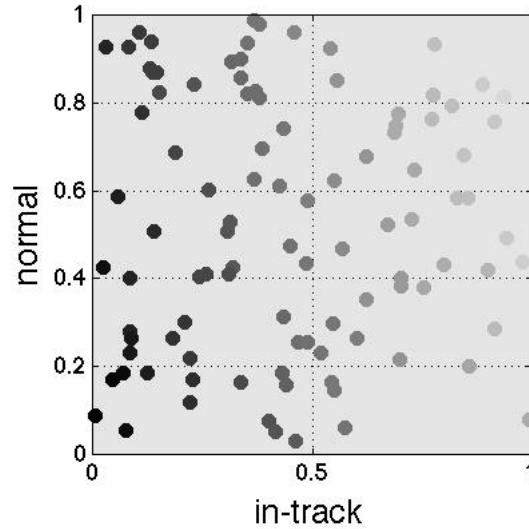
Figure 4.4. The probabilities for the fictitious example trend along normal vs in-track by decreasing in probability as the uncertainty gets closer to the maximums in each of the respective directions.

There is a trend in probability for the first type of plot and it is not immediately obvious how it is relevant. Looking at Figure 4.3, the trend seems to be in color from yellow to blue. However, looking at Figure 4.4, there is a trend in the normal uncertainty vs. the in-track uncertainty of the initial condition. In Figure 4.4, higher probabilities occur when the in-track and normal are both low in their respective ranges and visa versa. The trend is constant for all values of the out-of-plane uncertainty, which is out of the page. This is why Figure 4.3 trends from yellow to blue: the in-track and normal are both high when the probability is low, so the color is yellow. Some of the low probabilities are gray which is when the out-of-plane uncertainty is equally high. For the higher probabilities, when the in-track and normal are both low but the out-of-plane happens to be high, the dot is blue. Otherwise, if the out-of-plane is low as well, then the dot is black. Both these dots colors are seen for the higher probabilities. The color, in this sense, is a deterrent because it distracts the eye and doesn't immediately reveal the trend.

4.4 Case I

4.4.1 Background

Case I is based on 99942 Apophis (2004 MN4), or just Apophis, which is an interesting case because it has a turbulent history of impact probabilities.

It was first discovered in June 2004, lost shortly thereafter, and re-discovered in December 2004. The six month observation arc gave an impact probability of 0.4%, which is already very high. Subsequent observations in December only increased the likelihood of an impact on April 13, 2029. It reached an unprecedented impact probability of 2.7% when observations up to December 27th were included. Then, suddenly, with new pre-discovery observations from March 2004, the likelihood of impact in 2029 was almost entirely ruled out. Needless to say, the high probability of impact and the appreciable size of Apophis ($\sim$270 m) caused a significant scare in the asteroid tracking community and was reported to the public on NASA's Near Earth Object and the NEOdyS websites [28].

The story of Apophis exemplifies the uncertain nature of determining an asteroid's orbit and how the predictability of an asteroid's behavior is highly dependent on the number of observations available.

Although it is rather certain that Apophis will not impact the Earth in 2029, it will still make a very close approach, which will inevitably alter its current orbit significantly. The question now for Apophis is whether this close approach will put it into a newly perturbed orbit which has the possibility of impact in 2036. That is, if Apophis will pass through a keyhole[2] in 2029 which puts it into an impact scenario for 2036. The likelihood of this happening is low, and Apophis is still being studied with scrutiny.

4.4.2 Dynamics

Case I and Apophis share only their nominal position and velocity at epoch: July 23, 2010 00:00. This is the epoch for each the cases.

---

[2]A keyhole is the small region of space that encloses the initial conditions for a future impact scenario. If the asteroid passes through it, an impact will occur with higher probability on a future pass.

The orbit of Case I and the encounter regions generated by the three-body dynamics is shown in Figure 3.2. These encounter regions are representative of initial uncertainty range values of $a_1 = 1$ AU and $e = 2$. The value for a_1 is quite high. However, if a more realistic value were used in this simulation, on the order 10^{-6}, there would be no regions of encounter and the probability calculation could not proceed.

This point comes back to the dynamic model. Because the dynamic model is not accurate, even though Apophis itself makes a close approach to the Earth in 2029 on the order of 10^{-4} AU, the dynamic model in this study for Case I makes no such prediction, despite them sharing initial conditions. In fact, the solution found here never gets closer to the Earth than 0.05 AU and the uncertainty doesn't grow to a size large enough to cause an encounter region. So, the uncertainty is chosen to be large initially, to compensate for the deficient dynamic model.

4.4.3 Probability Results and Analysis

The total probabilities for Case I from the Monte Carlo simulation are presented in Figure 4.5. The date is effectively meaningless in this context because the dynamic model is not accurate. The date serves only to separate and identify the encounters from one another.

Each run of the calculation from integration of the equations of motion through Monte Carlo simulation to integration of the pdf (this process is referred to from now on as "the simulation") produces identically colored dots at different dates and values of probability. There are, in principle[3], dots of 100 different colors.

It is interesting to note that over all 100 runs of the simulation that produced randomly different initial uncertainties, the encounters are essentially the same across the board. Each run produced one data point in an encounter, but over all the runs, there are distinct groups of data points. This is analogous to the electron two-slit experiment in physics where separate runs of the experiment result in a placement of the electron on seemingly unrelated places on the detector, but over enough runs, a pattern emerges to which each particle adheres. After only one

---

[3] "in principle" for two reasons: in the practice of random numbers there can be repeats, and in the RGB color, there are not enough distinct colors to uniquely value each initial ellipsoid, but it is distinct enough to notice trends in the data.
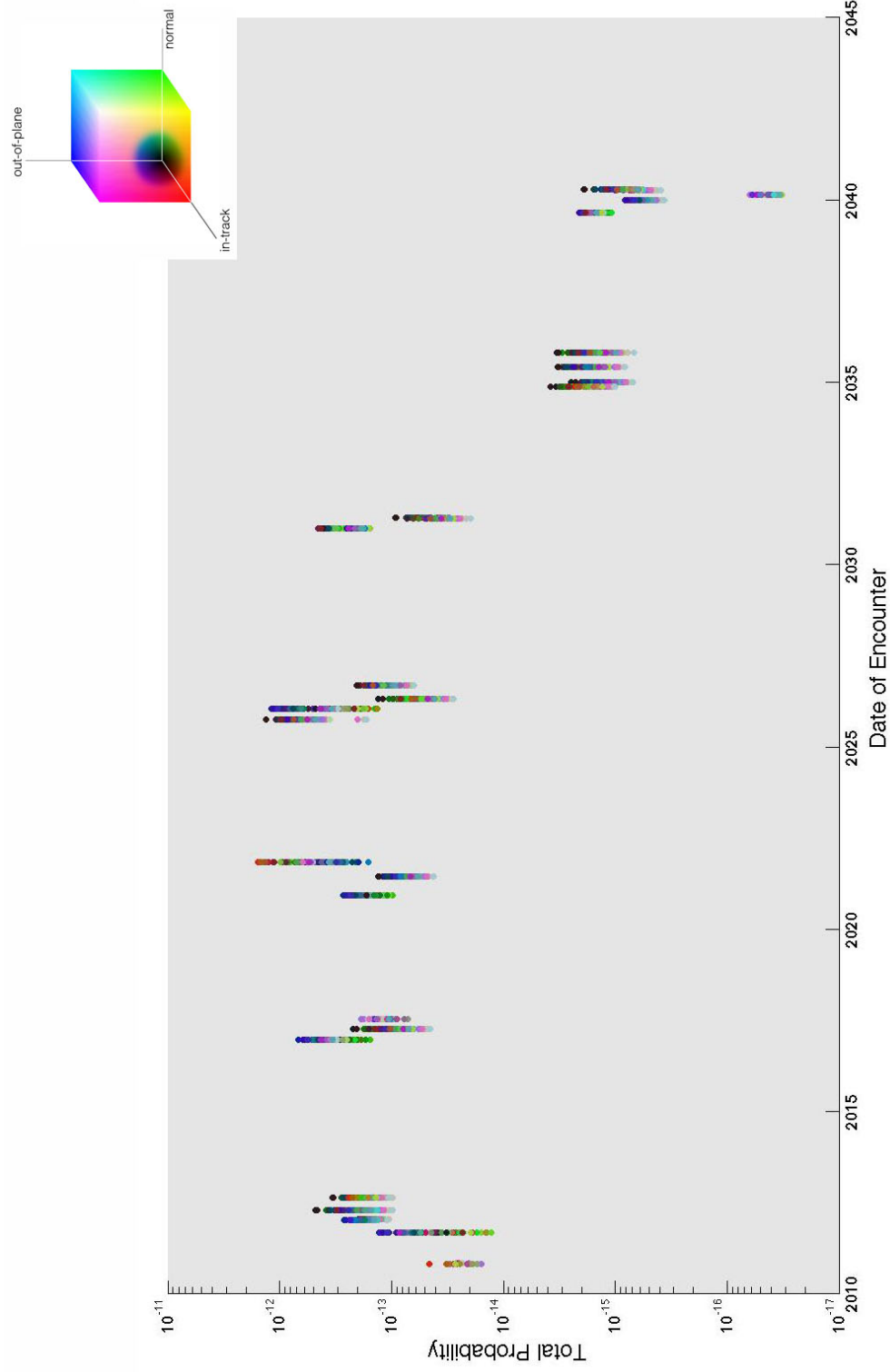
Figure 4.5. The total probabilities of Case I as a result of a Monte Carlo simulation and the methods discussed in Chapters 2 and 3. The color of each dot represents the relative size (in the respective range) of the in-track, normal, and out-of-plane dimensions of the initial uncertainty ellipsoid. See Figure 4.1.

Monte Carlo run, the total probabilities are spread over the date vs. probability space in a seemingly unrelated way, but after 100 runs, it is clear that probabilities only appear in specific places: the distinct encounters.

The relationship between initial uncertainty and the encounter regions for Case I is not continuous, so that little changes in uncertainty do not translate to large changes in the encounter dates. Rather, the relationship is more discrete so that each encounter corresponds to a range of uncertainties.[4] Different encounters are produced by different uncertainties, but the set of different possible encounters from the range of uncertainties available is finite and small. This means that the major contributor to the set of encounters is the dynamic model and initial conditions, or rather, the asteroid case that is being studied.

There is no trend over all the encounters associated with which dimension of the initial uncertainty ellipsoid is closer to the maximum value. That is, from top to bottom of Figure 4.5 there is no trend in color. Along a horizontal line that cuts across the encounters, several different colored dots appear. The trend in color is seen on an individual encounter basis. Each encounter is a set of vertically aligned dots. The encounters can be separated into two categories. The first category consists of those encounters that follow the following trend in the size of the initial uncertainty: higher probabilities are darker colored dots and lower probabilities are lighter (in a given encounter), which translates to higher probabilities resulting from smaller initial uncertainty and visa versa. The second category consists of those encounters that do not follow this trend.

From Figure 4.5 is can be seen that the majority of the encounters are in the first category. Further, those in this category have the same trend in color from top to bottom of the vertical line of dots. The lowest probabilities are a light shade of gray, which means that the initial uncertainty is close to the maximum in each direction: in-track, normal, and out-of-plane. The next higher probabilities are a light shade of red which means that while all the initial uncertainties are close to their maximums, the the in-track is slightly closer. The highest probabilities are a dark shade of green, which means that the uncertainty in the normal direction is the largest, but still low in its range.

---

[4]A continuous relationship is also known as one-to-one.

The encounters in the second category for Case I, for the most part, also have a trend. The lowest probabilities are almost pure green, while the highest probabilities are almost pure blue. This corresponds to the lowest probabilities having the normal direction of the initial uncertainty that is close to its maximum while the other two directions are close to their minimums, and the higher probabilities having the out-of-plane uncertainty closer to its maximum while the other two are lower. There are a few exceptions in this category, most notably the one on 11/1/2021 in which the trend in color is clearly from blue to red.

The trend of the first category is shown in the second type of plot in Figure 4.6. Here the trend is clearly visible: darker colored dots (higher probability) are clustered near the origin. Looking at Figure 4.7 it is apparent that the second category of encounters follows a trend similar to that in Section 4.3 where the trend is hidden. That is, the trend is only in the normal vs. in track uncertainties.
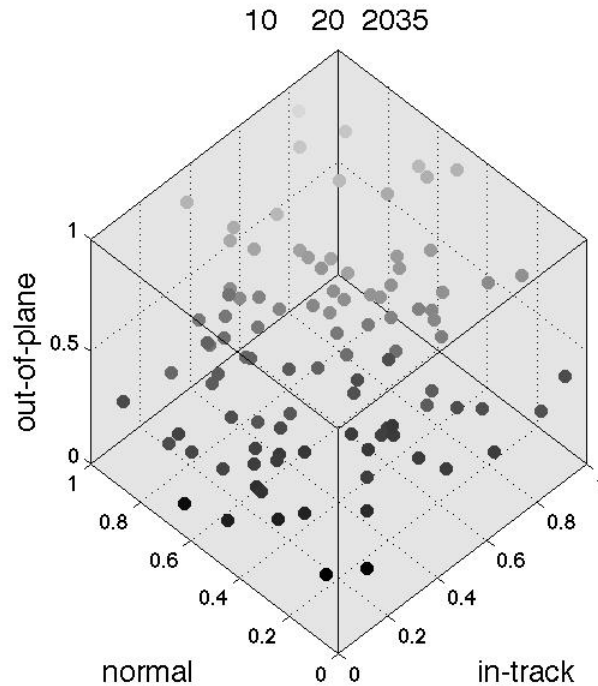
Figure 4.6. The probabilities of Case I for the encounter on 10/20/2035 trend from higher to lower as the uncertainty grows in all three directions. This falls into the first category of encounters.
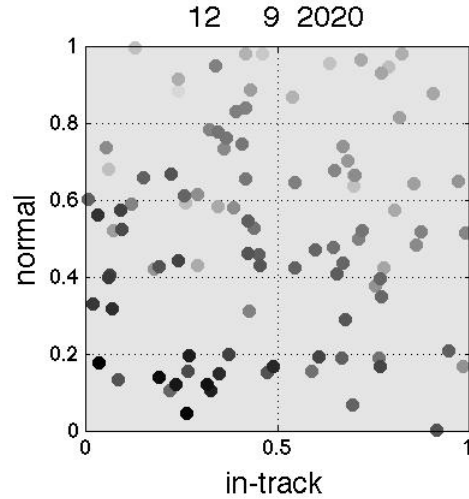
Figure 4.7. The probabilities for Case I for the encounter on 12/9/2020 trend from higher to lower in normal vs in-track. This falls into the second category of encounters.

To summarize Case I, the encounters are split between two categories with the majority having the trend of higher probabilities having lower initial uncertainties while the lower probabilities have higher initial uncertainties. The fraction of encounters that fall into the first category is about 4 out of 5. The second category is further spit into those that have a trend in color from green to blue and those that do not. From Figure 4.7, the trend is actually similar to the first category of encounters but only in normal vs in-track.

In one hundred runs of the simulation, each simulation having between 21 and 25 encounters, there are a total of 2274 data points. As seen in Table 4.1, these points occur in 25 distinct encounters (distinct, meaning differing by at least fifteen days). Twenty-one of these encounters occur in all 100 runs of the simulation. In other words, twenty-one dates in Figure 4.5 have 100 data points. One of the remaining four occurs in 90 runs, two occur between twenty and thirty times and one occurs less than five times. For example, the encounter on 4/11/2017 occurs in all 100 runs, while the next encounter on 7/12/2017 only occurs in 29 runs. The purpose of Table 4.1 is to show that the data points group into a small number of encounters despite the variety of differing initial conditions.

The dates in Table 4.1 are halfway points of the encounter, so that there is equal time before and after the date that is still the same encounter. The table does not include the length of the encounter, but the encounters range between 1

and about 40 time steps, where a time step is about half a day.

Results are presented for two other asteroid cases.

Table 4.1. The encounters of Case I that are distinct by fifteen days and their frequency. The full list of encounters is found in Appendix E.1. The date for the encounter throughout this study is unique to the dynamic model used here; in this context is only an identifier.

Encounters			Frequency
Month	Day	Year	
11	1	2010	25
9	6	2011	90
1	14	2012	100
4	15	2012	100
8	23	2012	100
12	18	2016	100
4	11	2017	100
7	12	2017	29
12	9	2020	100
6	9	2021	100
11	1	2021	100
9	30	2025	100
1	16	2026	100
4	25	2026	100
9	11	2026	100
12	30	2030	100
4	10	2031	100
11	16	2034	100
12	29	2034	100
6	2	2035	100
10	20	2035	100
8	28	2039	100
12	31	2039	100
2	21	2040	30
4	10	2040	100

4.5 Case II

4.5.1 Background

Case II is based on 1999 RQ36, which was discovered in 1999 by the LINEAR observatory. It has been observed throughout the last decade.

RQ36 is interesting because it has a fairly high rating on the Palermo Scale, which assesses the over all risk posed by a given asteroid. The impact probability is currently about 0.07% in the last half of the 22nd century, which is fairly high.

The asteroid RQ36 "has the lowest uncertainty, [at the epoch 8 June 2001], in semi-major axis of any asteroid." But, this minimum uncertainty ignores the dynamics of the Yarkovsky effect, which is an outgassing from the asteroid due to heat from the Sun. This effect can have a large influence on the future motion of the asteroid and if not taken into account can cause as asteroid to be lost. The problem is that the physical attributes of the asteroid that lead to the Yarkovsky effect are, for the most part, unknown. Nevertheless, there are techniques available for modeling this effect [29].

4.5.2 Dynamics

Figure 4.8 shows the orbit of Case II and a typical set of encounters. The range values are also $a_1 = 1$ AU and $e = 2$.

4.5.3 Results

The first type of plot of probabilities for Case II is Figure 4.9. Like Case I, there is no absolute trend in probability: the trends are on an encounter basis. Also like Case I, the encounters can be split into two categories. The fraction of encounters that fall into the first category is again about 4 out of 5. The trend for the first category is identical to that for Case I. The lowest probability in each encounter is a shade of gray and the highest is a shade of green and the pattern of dots in between is similar to that of Case I. However, the second category in Case II does not have the same trend in color as in Case I.

Figure 4.10 shows the trend from lower uncertainty to higher uncertainty for the first category of encounters. While the second category for Case II does not

have the same color trend as for Case I, the trend in initial uncertainty is actually quite similar to Case I. This is shown in the second type of plot for Case II in Figure 4.11.

Each simulation in 100 runs has eleven encounters or, put another way, each encounter occurs in all 100 runs. Table 4.2 shows the dates of the eleven encounters.
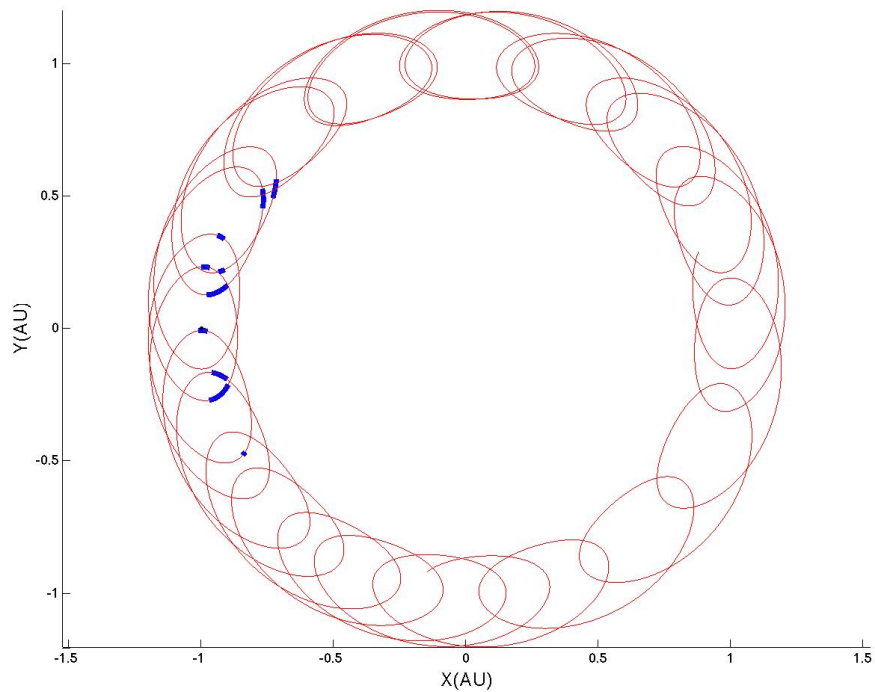
Figure 4.8. The orbit and typical encounters of Case II as predicted by CR3BP. The Earth is near (-1,0).
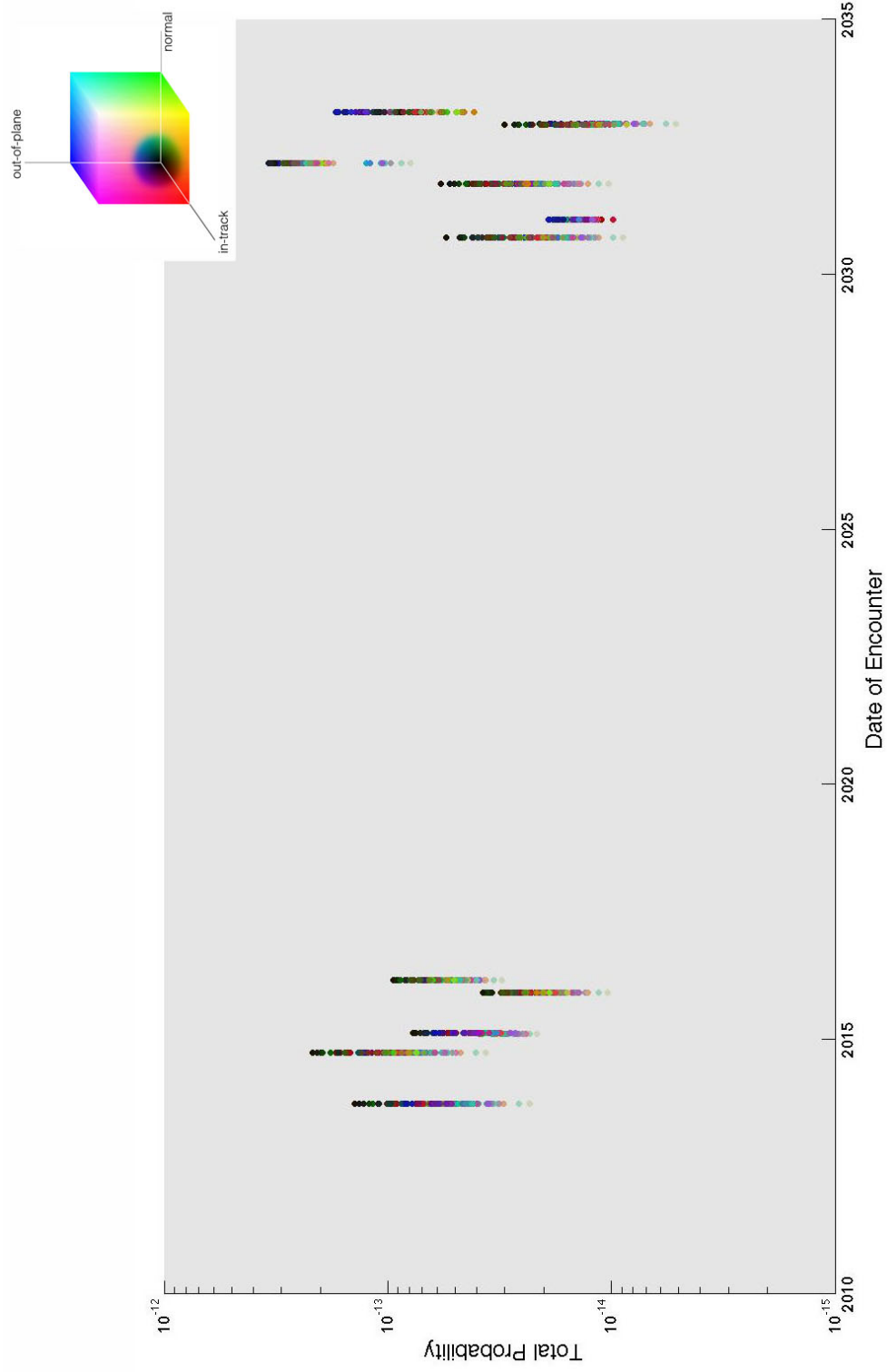
Figure 4.9. The total probabilities of Case II. A red dot signifies the initial in-track uncertainty is closer to its maximum, a green dot corresponds to the normal direction and a blue dot corresponds to the out-of-plane direction.
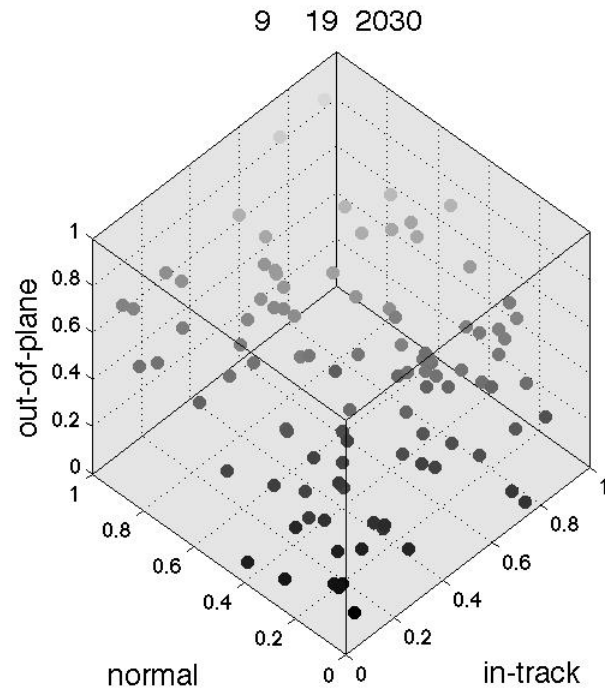
Figure 4.10. The probabilities of Case II for the encounter on 9/19/2030 trend from higher to lower as the uncertainty grows in all three directions. This falls into the first category of encounters.
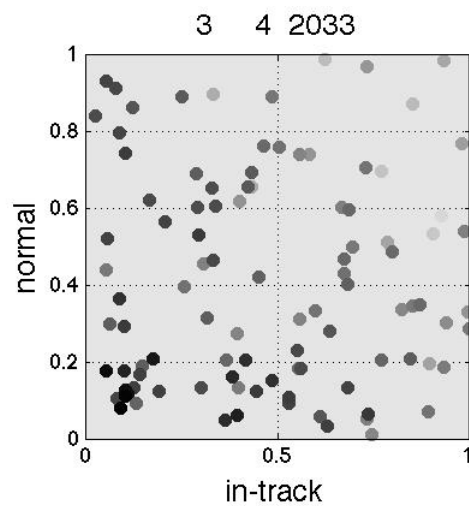
Figure 4.11. The probabilities for Case II for the encounter on 3/4/2033 trend from higher to lower in normal vs in-track. This falls into the second category of encounters.

Table 4.2. The encounters of Case II that are distinct by fifteen days and their frequency. The full list of encounters can be found in Appendix E.2.

Encounters			Frequency
Month	Day	Year	
9	25	2013	100
9	27	2014	100
2	9	2015	100
11	27	2015	100
2	29	2016	100
9	19	2030	100
1	29	2031	100
10	12	2031	100
3	8	2032	100
12	11	2032	100
3	4	2033	100

4.6 Case III

4.6.1 Background

Case III is based on 2010 RF12, which made headlines in September 2010 when it and other small asteroid 2010 RX30 made very close approaches within hours of one another. The two objects were discovered only a few days prior, but with collaboration around the globe, their orbits were determined and the prediction of their close approaches was made. It was one of a handful of times that the orbits of asteroids that have activity near the Earth were first observed and predicted in only a few short days. RF12 is thought to be only several meters in diameter, so a collision would not be disastrous, but by studying this case, the methods for impact probability calculation can be further developed and tested, so that when we encounter an asteroid that does pose a significant threat, the techniques are properly refined.

4.6.2 Dynamics

The orbit and encounters of Case III as predicted by the CR3BP is seen in Figure 4.12. The range values that contributed to these encounters are $a_1 = 1$ AU and
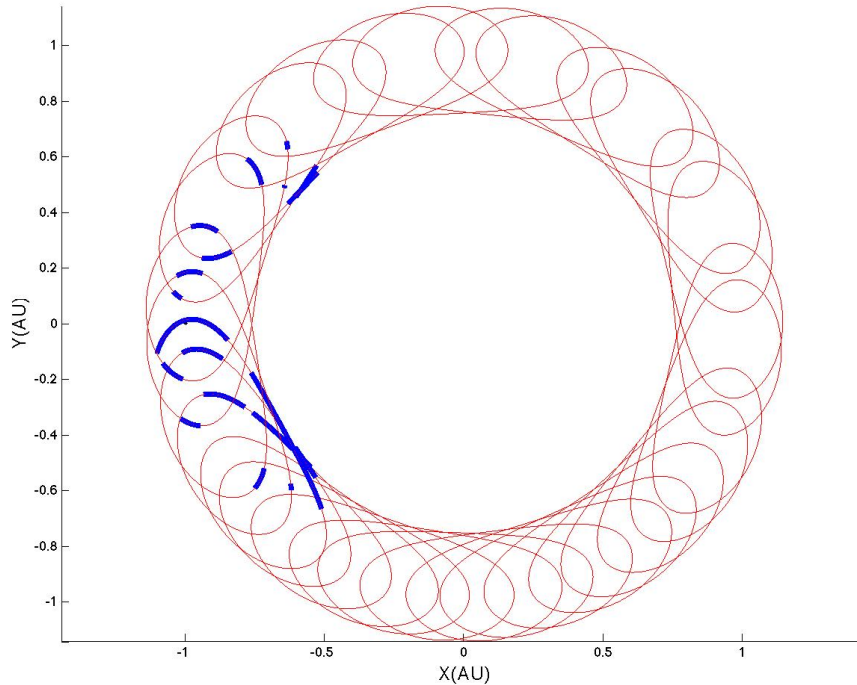
Figure 4.12. The orbit over a 30 year integration and typical encounters of Case III as predicted by CR3BP. The black dot representing the Earth near (-1,0) is not to scale.

$e = 2$. Case III, unlike Case II, has a long encounter for its close approach. This is because this close approach happens near the initial epoch and the uncertainty is still aligned with the velocity vector. Recall that the initial epoch is in July of 2010, so this is near to the path that RF12 took in September 2010.

The orbit of Case III is similar to that for Case I and Case II. The asteroid makes loops that advance in a circle around the Sun. The difference is that the outsides of the loops swing upwards in the z-direction for Case III whereas they dip downwards for Case I and Case II. Figure 4.13 conveys this for each case. This happens because of the characteristics of the orbit in the inertial frame. Each case is based on a real asteroid and the real asteroids are on inclined (to the ecliptic), Earth crossing orbits. For Apophis and RQ36, the apogee of the orbit is below the ecliptic, while for RF12 it is above the ecliptic. Or also, the eccentricity vector points above the ecliptic for RF12 and below for Apophis and RQ36. These are reflected in the cases, respectively, so that when Case I is inside Earth's orbit
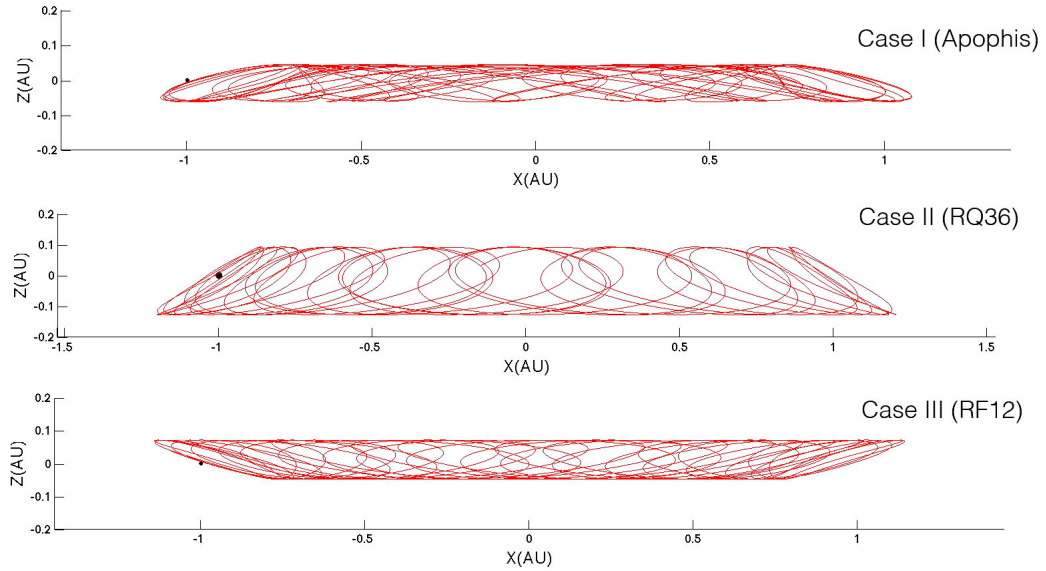
Figure 4.13. The orbits of the three cases projected on the x-z plane. The cone or bowl shape of the orbit is representative of the inclination of the orbits in the inertial frame and are correct for the corresponding real asteroids upon which the cases are based.

(closer to the origin), the orbit is higher, and visa versa. Also note that Case II appears to be the most inclined of the three, which is true for RQ36. While the dynamic model produces an inaccurate nominal solution, it is close enough to reality to have these gross characteristics. This demonstrates the validity of the three-body dynamics.

4.6.3 Results

The first type of plot for the probabilities for Case III is Figure 4.14. Again, the runs organize by encounters and there is no absolute trend. The encounters can be split into the two categories with encounters in the the first category occurring 2 out of 3 times. The first category in Case III follows the trend of Case I and Case II that can be seen in the first type of plot, while the second category holds no trend similar to either Case I or Case II nor does a majority of the encounters in the second category for Case III have the same trend.

Figure 4.15 confirms the trend for the first category. Figure 4.16 shows the second type of plot for the second category which has the same type of trend as for Case I and Case II.
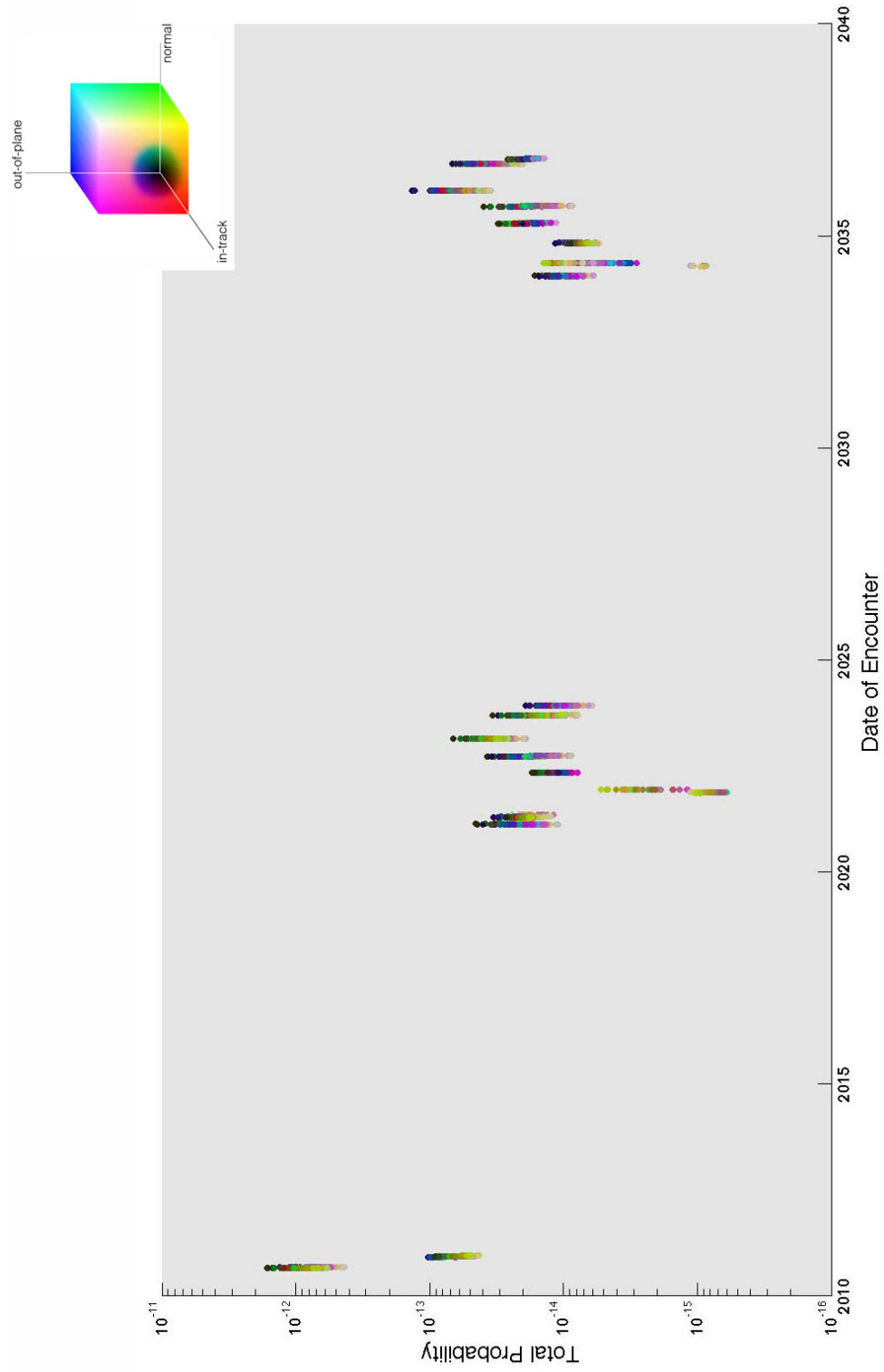
Figure 4.14. The total probabilities of Case III. These values are not comparable to probabilities calculated by other methods for 2010 RF12.
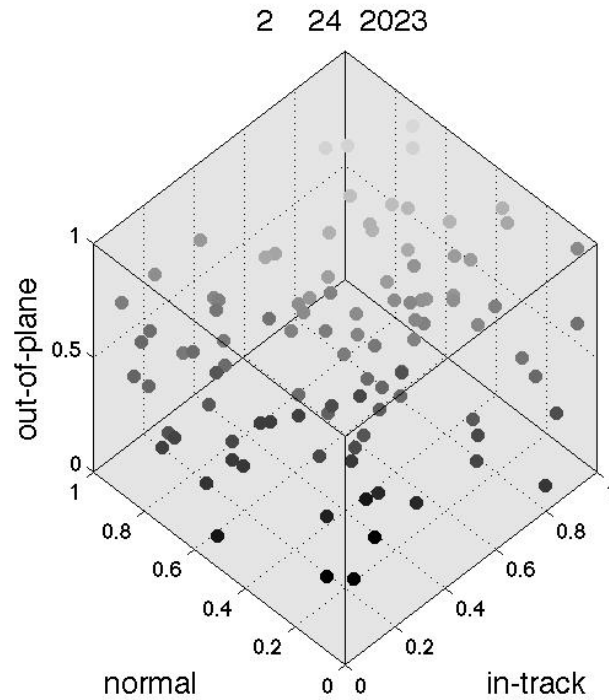
Figure 4.15. The probabilities of Case III for the encounter on 2/24/2023 trend from higher to lower as the uncertainty grows in all three directions. This falls into the first category of encounters.
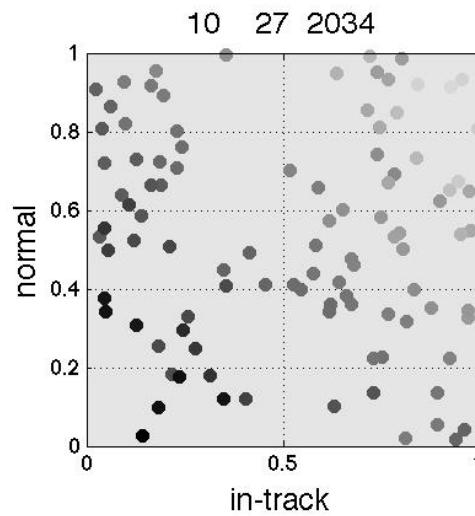
Figure 4.16. The probabilities for Case III for the encounter on 10/27/2034 trend from higher to lower in normal vs in-track. This falls into the second category of encounters.

This case has a total of 1808 data points in 21 encounters distinct by fifteen days (Table 4.3). Sixteen occur all 100 times, one occurs 99 times, while the remaining four happen less than 50 times.

Table 4.3. The encounters of Case III that are distinct by fifteen days and their frequency. The full list of encounters can be found in Appendix E.3.

Encounters			Frequency
Month	Day	Year	
9	2	2010	100
12	2	2010	100
2	18	2021	100
4	14	2021	100
5	9	2021	17
11	13	2021	44
12	13	2021	38
5	1	2022	100
9	24	2022	100
2	24	2023	100
9	8	2023	100
12	2	2023	100
1	20	2034	100
4	14	2034	10
5	9	2034	99
10	27	2034	100
4	17	2035	100
9	11	2035	100
1	28	2036	100
9	13	2036	100
10	23	2036	100

4.7 Summary

4.7.1 Dynamics

Based on the real initial conditions of the asteroids position and velocity, the three-body problem reproduced orbits that resemble the true orbit in its gross characteristics. For example, Case III (based on RF12) is an Earth crossing asteroid, which means that its eccentricity vector points in the direction of the orbit

that is inside Earth's orbit. It also has an eccentricity vector that points below the ecliptic. This would mean that its orbit in the rotating frame, with the Earth fixed, would resemble the top inside rim of a bowl, or that looking down the z-axis, is concave. This is in fact what is produced by the implementation of the three-body problem here. Conversely, Case II (based on RQ36) has its eccentricity vector pointing above the ecliptic, which would mean that its orbit in the rotating frame would be—looking down the z-axis—convex. This, also, is produced by the dynamic model here.

The dynamic model for this study also predicts close approaches for each of the cases. Where they deviate from the real asteroids they are based on are the particular date of the close approach and the close approach distance. This is what is meant in Chapter 2 by the inaccuracies of the model. The orbit is not exact, but for the purposes here, is the proper backdrop for the probability analysis.

4.7.2 Probability

The Cases are called I, II, and III in order to separate them from the real asteroid upon which they are based. The probabilities calculated here do no reflect actual risk posed by the real asteroids. While the initial conditions are real, the dynamic model is simplified and the initial uncertainty is unrealistic. So the encounters and probability are essentially arbitrary. Nevertheless, the relative trend in probability and initial uncertainty is still valid: it is exemplary of the method used to calculate probability. This method can be applied to real asteroids if a true dynamic model and initial uncertainty are employed.

The trend in probability for Cases I, II, and III can be summarized as follows. The encounters in the first category trend the same by all three directions of the initial uncertainty for all three cases. That is, lower initial uncertainties lead to higher probabilities and visa versa. The second category according to the first type of plot (the color plots) does not hold the same trend across cases. The trend is in fact revealed to be the same across cases (and similar to the first category) by the second type of plot, which takes the color out of the display. The first type of plot is necessary to see how the different runs with differing initial uncertainties produce the same small set of encounters.

For all encounters over all three cases, the statement can be made that initial uncertainties that are closer to the minimum in at least two principal directions produce higher probabilities of impact.

For the fictitious case of the asteroid on a collision course, it is found that this method of calculating probability properly predicts a significantly higher probability of impact as expected. Also, the probabilities trend similarly to those for the three cases.

In the next chapter, the results are explained by a simple example and the contributions and limitations of this thesis are discussed. Also, suggestions are made about the work that can follow from this study.

Chapter 5

Conclusions

This thesis has examined how the variability of initial uncertainty effects the total probability calculated by a method that differs from standard practices of asteroid impact probability calculation. This differing method was developed in Chapter 3 and applied to asteroid cases that utilized the dynamics developed in Chapter 2. In Chapter 4, the trend in the calculated probability vs. initial uncertainty was revealed. This chapter describes the source of this trend and looks at the results from a perspective that takes into account the realistic interpretation of the initial uncertainties and the resulting probabilities of impact. Also, this chapter makes recommendations for future work.

5.1   Summary of Contributions

A major contribution of this thesis is the development of an alternative method for impact probability calculation using the positional uncertainty ellipsoid as the central tool. As an application of this method, a Monte Carlo simulation was run to find a relationship between initial uncertainty and total probability. The trend found is another contribution. To show how this trend is achieved, two one-dimensional probability density functions are examined in more detail and their relationship is applied to the three-dimensional case of positional uncertainty.

5.1.1 Explanation of the Trend

To see how the trend found is what is expected, the parameters of the problem must be classified and the variables that contribute to the trend are highlighted.

The encounters are the same for each run of the simulation for a given asteroid. This means that the relative Earth vector is the same for each calculation of probability at that encounter. The dynamics that produce the uncertainty during the encounter are also the same. Further, the orientation of the initial uncertainty is fixed so that the uncertainty throughout the encounter has a one to one relationship with the initial conditions that produced them. Also, larger initial conditions will produce a larger propagated uncertainty at a given future time. The only variable in this problem is the size of the initial uncertainty. Because the relationship between initial uncertainty and propagated uncertainty is one-to-one, this can be translated to the only variable being the size of the uncertainty during the encounter. Because the encounter is the same distance away from the Earth for each run of the simulation, the only variable to affect probability is the size of the uncertainty during the encounter.

Now, the probability calculated is an integration of the probability density function, which is a represented by the size of the uncertainty. Figure 5.1 shows two probability density functions with different standard deviations, σ. The vertical
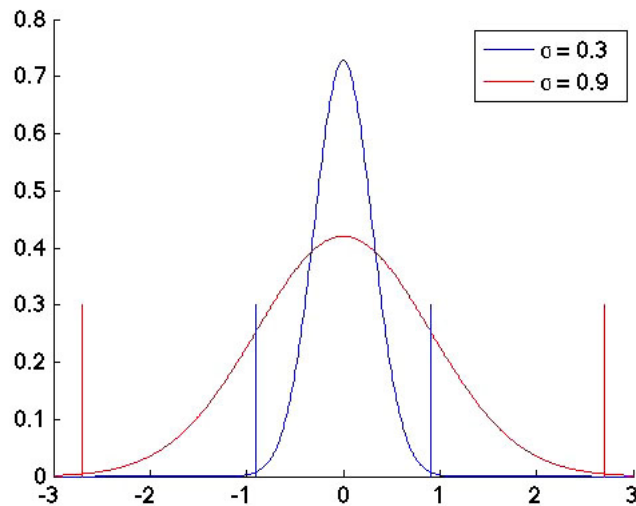
Figure 5.1. Two pdfs with differing standard deviations.

lines indicate 3σ. Near the mean, the pdf is greater when the standard deviation is lower (blue is greater than red). Farther from the mean, the larger standard deviation has a greater pdf (red is greater than blue). The distance below which the blue pdf is greater than the red pdf is found by equating the two pdfs and solving for the distance from the mean, s.

$$s = n\sigma\sqrt{\frac{2\ln\sqrt{n}}{n^2 - 1}} \tag{5.1}$$

where $n\sigma$ is the greater standard deviation. For the standard deviations in Figure 5.1, according to equation (5.1), $s = 0.334$. For the probabilities to be greater when 3σ is smaller, as is seen in the results, the Earth must be less than the distance s from the center of the uncertainty ellipsoid at the time of the encounter. This is in fact the case for the three asteroid cases in this study: the 3σ uncertainty can grow to be more than 300 AU, $n = e = 2$, so from equation (5.1), $s \approx 48$ AU while the Earth is at most about 2 AU from the center of the ellipsoid. This is why the probabilities are greater when the uncertainty is tighter: the tighter uncertainty has a greater pdf at the position of the Earth.

This explanation is based on the one-dimensional case. The pdf that is uncertainty is three-dimensional. It is one of the contributions of this thesis to show that this trend is maintained for higher-dimensional pdfs in the scenario of asteroids in orbit around the Sun. Also, it is shown in Section 4.3 that this method produces the expected significantly higher probabilities for an asteroid on a direct collision course with the Earth.

5.1.2   Results in Perspective

A higher probability is desired because the probability of impact should be a conservative estimate at best. It would not be beneficial to calculate true probabilities that are deceptively low, giving us a false sense of security. With the advancement of ever more accurate observational and theoretical techniques to determine orbits of asteroids, the uncertainties will diminish (however, they will never vanish).

This leads to the optimistic conclusion that the probabilities calculated in the future will always be greater than they are today. But, looking back at Figure 5.1,

this relationship between standard deviation and probability only holds near the mean. If the uncertainties shrink enough and the distance of the encounter stays constant, there is a range for which a smaller uncertainty has a lower probability.

The trend in probability found in this study was a result of the vastly large initial uncertainties, which led to the even larger propagated uncertainties. These propagated uncertainties are so large that the Earth is well within the distance s—the range for which the smaller uncertainty ellipsoid integrates to a higher probability. In no real sense would the initial uncertainty be 1 AU. It may grow to be that large after several decades of propagation, but an uncertainty of 1 AU today would mean that the asteroid is lost.

The probabilities calculated are extremely small. Even for the impact example in Section 4.3 the probabilities are not indicative of a very likely impact. The probabilities for the three cases are at the edge of what is considered negligible. The lowest probabilities calculated for PHAs by NASA's NEO website [5] are greater than the largest probabilities produced by the Monte Carlo simulations of this study. This is an indication that work must continue on this method before it can be applied to real asteroid cases.

So while the result is promising, it is given with the caveat that it was the result of unnaturally large initial uncertainties.

These large initial uncertainties are required because without them, no encounters occur. This highlights a fundamental limitation of this method as applied to real cases. The uncertainties in a real case would be orders of magnitude less than an AU. With uncertainties this small used to run the simulation, no encounters were detected and the probability calculation could not proceed.

5.2   Recommendations for Future Work

The recommendations given in this section are primarily concerned with refining the methods presented here so that they can be applied to real asteroids and produce actual probabilities. The first change to be made to do this is to use realistic initial uncertainties. So far, this is impossible, but recommendations to accommodate these impossibilities are given in Section 5.2.2.

5.2.1 Dynamic Model

As has been stated many times in this thesis, the dynamic model is intentionally left inaccurate for simplicity. In the future, it is formally recommended that the dynamic model is replaced with a more sophisticated model that produces what is considered the true trajectory of the asteroid. This will vastly increase the accuracy of the encounter regions and probabilities calculated.

To create a more accurate dynamic model, additional factors must be taken into account including perturbing bodies in the solar system, general relativity, and the Yarkovsky effect, among others.

5.2.2 Probability Calculation

The uncertainty being so large initially is the greatest limitation of this study. As was stated above, this is necessary to produce encounters over which a probability calculation can be performed. If this method is to be applied to real cases more realistic initial uncertainties are required.

More realistic initial uncertainty can be used if the propagation technique is adjusted. Remember that the uncertainty is propagated by a linear transformation of the state transition matrix. Over the time spans of the desired propagation (30 years or greater), the linear assumption may not always hold. It is recommended that nonlinear propagation of uncertainty is investigated in order to open the possibility of starting with lower initial uncertainties. Nonlinear propagation may lead to faster growth of the uncertainty, which would lead to more regions of encounter as defined here.

The goal of any future work is to achieve actual probabilities of impact of asteroids with the Earth. By using realistic uncertainty, the probabilities calculated will also be more realistic. Methods to nonlinearly propagate the uncertainty are addressed by Chesley [30] and together with the methods discussed in the preceding chapters could lead to more realistic probabilities of impact.

Appendix A

Scripting Techniques

A.1   Solving the EOMs

In MATLAB, two scripts are needed to integrate the equations of motion: a main script and a function script. The main script contains the definitions of all constant quantities including the initial conditions and time span of the calculation. The main script also contains a statement that passes these quantities to the solver itself. The function script contains the equations of motion the form of which is altered to accommodate the solver (see Section 2.3). The function is an object defined by this script that is then passed in the main script to the solver, ode45 [31], a Runge-Kutta 4/5 variable step size integrator.

   With a minimum of two scripts, the Newtonian equations of motion are solved and the nominal solution of the asteroids trajectory is obtained.

A.2   Propagating the Planets

An embedded function is needed to numerically solve for the positions of the perturbing bodies at each time step. The statement calling the embedded function and solving for it using the standard solver is placed inside the first function (which is solving the equations of motion of the asteroid itself) and before the lines defining equation (2.11) so that the positions of the perturbing bodies are available. The embedded function is then equation (2.19) for each of the perturbing bodies, k. The return of the embedded function is a 3×N matrix of all the positions of the perturbing bodies at that time step.

Covariance Propagation

Linear propagation of the uncertainty is achieved by a transformation on the initial covariance matrix [32].

$$P = \Phi(t, t_0) P_0 \Phi^T(t, t_0) \tag{B.1}$$

This can be understood in the following way. The State Transition Matrix is defined as:

$$\Phi = \frac{\partial X}{\partial X_0} \tag{B.2}$$

where X is the state vector. The initial normal (or information) matrix, which is the inverse of the covariance matrix, is defined as:

$$C_0 = \left(\frac{\partial \xi}{\partial X_0} \right)^T \left(\frac{\partial \xi}{\partial X_0} \right) \tag{B.3}$$

and the corresponding normal matrix at any time t is:

$$C = \left(\frac{\partial \xi}{\partial X} \right)^T \left(\frac{\partial \xi}{\partial X} \right) \tag{B.4}$$

where ξ is the observational residual. Applying the chain-rule to these differentials gives,

$$C = \left(\frac{\partial \xi}{\partial X_0} \frac{\partial X_0}{\partial X} \right)^T \left(\frac{\partial \xi}{\partial X_0} \frac{\partial X_0}{\partial X} \right) \tag{B.5}$$

then by distributing the transpose,

$$C = \left(\frac{\partial X_0}{\partial X}\right)^T \frac{\partial \xi}{\partial X_0}^T \frac{\partial \xi}{\partial X_0} \left(\frac{\partial X_0}{\partial X}\right) \tag{B.6}$$

the information matrix comes out of the middle two terms,

$$C = \left(\frac{\partial X_0}{\partial X}\right)^T C_0 \left(\frac{\partial X_0}{\partial X}\right) \tag{B.7}$$

The inverse of this equation then gives,

$$P = C^{-1} = \left(\frac{\partial X}{\partial X_0}\right) P_0 \left(\frac{\partial X}{\partial X_0}\right)^T \tag{B.8}$$

Here is it clear that equation (B.8) with (B.2) is identical to (B.1) [18].

It should be noted here that the linear assumption used here to propagate the uncertainty can fail in certain cases. Examples include when the time span of propagation is especially long or when the asteroid makes a close approach. In these cases, nonlinear propagation is necessary, but can be increasingly computationally taxing [30]. Methods involving nonlinear propagation are outside the scope of this thesis and are discussed further in the section on future work.

Linear Approximation

This appendix is a summary of [33].
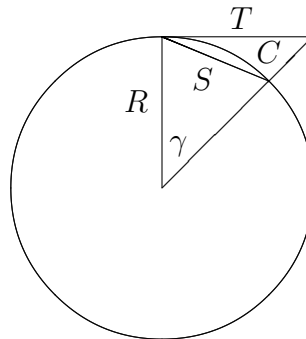
Figure C.1. A circle with a secant and tangent.

The question is what maximum angular arc of a circle can be approximated by a straight line. To answer this, two relative errors are examined: that of the secant, S, associated with the arc, C, and the tangent, T, that is coincident with the arc. See Figure C.1. These errors are denoted ϵ^* and ϵ^{**}, respectively.

If the radius of the circle is R, then the length of the arc is

$$C = R\gamma \tag{C.1}$$

Also, the length of the secant is

$$\frac{S}{2} = R \sin\left(\frac{\gamma}{2}\right) \tag{C.2}$$

Then the relative error is,

$$\epsilon^* = \frac{S - C}{C} = \frac{2}{\gamma} \sin\left(\frac{\gamma}{2}\right) - 1 \tag{C.3}$$

With an angle of 0.1 radians, the error is 0.04%. This is sufficiently smaller than one.

The length of the tangent is

$$T = R \tan\gamma \tag{C.4}$$

So that its error is,

$$\epsilon^{**} = \frac{T - C}{C} = \frac{1}{\gamma} \tan\gamma - 1 \tag{C.5}$$

With an angle of 0.1 radians, the error is 0.3%. This is sufficiently smaller than one as well.

So, with $\gamma = 0.1$ rad (5.8°) there is close agreement between a straight line and a circular arc.

Appendix D

Encounter Region Check

The check whether the Earth is inside the uncertainty ellipsoid is performed at each time step along the orbit and can be done in several ways.

The encounter region is defined as the region along the orbit when the Earth is inside the uncertainty ellipsoid. Of course, "the Earth" refers to the surface of the Earth because that is where collisions occur. However, at the distance scale of an asteroid in obit around the Sun, as in the three asteroid cases in Sections 4.4 - 4.6, it is usually sufficient to treat the Earth as a point located at its center. Methods that do this are discussed in Appendix D.1. Only when doing analysis very close to the Earth, when the size of the Earth is significant compared to the length scale, as in Section 4.3, is it necessary to include the extent of the Earth when determining the encounter regions. A check for close approaches will tell whether it is necessary to include the size of the Earth even when dealing with large distance scales. A technique to take into account the extent of the Earth is addressed in Appendix D.2.

D.1 Earth as a Point

D.1.1 Cartesian

The surface of the uncertainty ellipsoid in Cartesian coordinates is subject to the following condition

$$\begin{bmatrix} x' & y' & z' \end{bmatrix} P^{-1} \begin{bmatrix} x' \\ y' \\ z' \end{bmatrix} = 1 \tag{D.1}$$

where P is the 3×3 covariance matrix and $[x'\ y'\ z']$ are coordinates centered at the ellipsoid. To determine whether a position is inside this ellipsoid, one takes the inequality less than or equal to one.

D.1.2 Spherical

Alternatively, one can determine the spherical angles that the relative position vector of the Earth with respect to the center of the ellipsoid makes with the ellipsoid's principal axes, $[x'\ y'\ z']$. These angles are shown in Figure D.1. To do this, first, take the dot product of the unit (x',y') components of the position with the x'-axis and then take the inverse cosine (a check of quadrant is required). This is the angle θ. Next, take the dot product of the (x',y',z') components of the position with the z'-axis and then take the inverse cosine (no quadrant check is required). This is the angle ϕ. The distance, d, from the center of the ellipsoid to its surface at the spherical location defined by these angles can then be calculated:

$$d = \sqrt{\left[\frac{\sin^2 \phi \cos^2 \theta}{\lambda_1} + \frac{\sin^2 \phi \sin^2 \theta}{\lambda_2} + \frac{\cos^2 \phi}{\lambda_3} \right]^{-1}} \tag{D.2}$$

where λ_i are the eigenvalues of the covariance matrix. Then one checks whether the magnitude of the relative position of the Earth from the center of the ellipsoid is less than or equal to d.

The cartesian and spherical checks, not surprisingly, produce identical encounter regions.
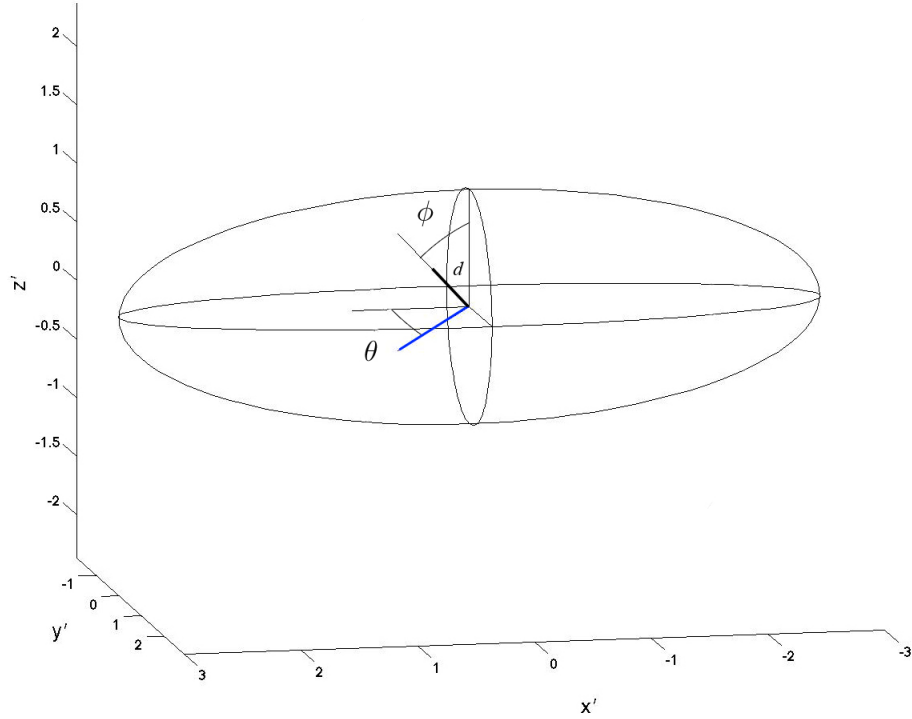
Figure D.1. The uncertainty ellipsoid in a frame aligned with its principal axes and the spherical angles that the relative Earth vector (the vector from the center of the uncertainty ellipsoid to the center of the Earth) makes with those axes. The thin black line is the relative Earth vector, the thick black line is the part of that vector inside the ellipsoid, and the blue line is the projection of the relative Earth vector onto the x′-y′ plane.

D.2   Earth with Extent

Taking into account the extent of the Earth is as easy as adding to the relative Earth vector a vector from the center of the Earth to its surface and then using the methods for determining whether a point is inside an ellipsoid. The difficulty is that this process requires checking the whole range of additive vectors at each time step and is very computationally intensive. A more efficient method is necessary.

The problem is determining when two ellipsoids intersect. The two ellipsoids are the uncertainty ellipsoid and the Earth (the Earth is an ellipsoid with three equal principal axes). Alfano [34] and Chan [35] develop the technique to do this.

The surface of an ellipsoid can be described by:

$$XTST^T X^T = 0 \tag{D.3}$$

where

$$X = \begin{bmatrix} x & y & z & 1 \end{bmatrix} \tag{D.4}$$

$$T = \begin{bmatrix} 1 & 0 & 0 & 0 \\ 0 & 1 & 0 & 0 \\ 0 & 0 & 1 & 0 \\ -x0 & -y0 & -z0 & 1 \end{bmatrix} \tag{D.5}$$

$$S = \begin{bmatrix} C_{11} & C_{12} & C_{13} & 0 \\ C_{21} & C_{22} & C_{23} & 0 \\ C_{31} & C_{32} & C_{33} & 0 \\ 0 & 0 & 0 & -1 \end{bmatrix} \tag{D.6}$$

where $[x0, y0, z0]$ is the center of the ellipsoid and C_{ij} are the elements of inverse of the characteristic matrix of the ellipsoid. In the case of the uncertainty ellipsoid, this characteristic matrix is the covariance matrix, P. C is called the information matrix:

$$C = P^{-1} \tag{D.7}$$

The two ellipsoids are then

$$XAX^T = 0 \tag{D.8}$$

and

$$XBX^T = 0 \tag{D.9}$$

By subtracting equation (D.9) from a scaled (D.8): $X(\lambda A - B)X^T = 0$, the problem becomes an eigenvalue problem. To get it in the recognizable form, left multiply the inner matrix by AA^{-1}.

$$XA(\lambda I - A^{-1}B)X^T = 0 \tag{D.10}$$

As explained by Alfano and Chan, the eigenvalues of $A^{-1}B$ are indicative of the state of intersection of the two ellipsoids described by A and B. When two of

the eigenvalues are negative and unequal, the ellipsoids are not intersecting. When the two eigenvalues are negative and repeating, the two ellipsoids are just touching (at a single point). When the two eigenvalues are complex conjugates, one end of one ellipsoid is inside the other. When the two eigenvalues are positive, the two ellipsoids are intersecting through one another.

Because there are four eigenvalues for this problem, Alfano refers to admissible and inadmissible eigenvalues. One example of an inadmissible eigenvalue is one with an eigenvector with a zero in the last component. This is inadmissible because "this formulation has been framed in a four-dimensional space with the last dimension fixed [34]" as shown in equation (D.4). It is not clear whether this is the only case of inadmissibility.

In any case, when applying this method to the problem here, it is found that the eigenvectors do not behave as described by Alfano and the eigenvalues cannot be distinguished between admissible and inadmissible. This is not actually a problem because the classification of the eigenvalues can be applied even when all four are taken equally.

When any of the four eigenvalues are complex conjugates, the ellipsoids are overlapping, when all four are positive, they are overlapping, when any two are negative and equal they are touching, when any two are negative and unequal, they are separate.

With this check on the eigenvalues of $A^{-1}B$, the regions along the orbit of the asteroid when the instantaneous uncertainty ellipsoid and the sphere of the Earth intersect can be determined. This works whether A or B is the Earth.

E

List of Encounters

The "distinct value" in Chapter 4 of 15 is chosen because the encounters of all three cases are not perfectly discrete. The characteristic of being discrete or continuous is a spectrum, so that some cases are more continuous than others.

Small changes in the initial uncertainty does produce small changes in the mean date of an encounter. So over all the simulations in a case, there are several encounters that appear only once or twice that are only a day or less different than other encounters in other simulations.

This Appendix presents all the encounters of each case to the resolution of the numerical results: half a day.

E.1   Case I

There are 68 encounters that are distinct by half a day. The greater-than/less-than split at 50 is 20/48. Six encounters appear only once.

While these encounters are more continuous, they are still grouped around a specific date with gaps in time between them. The date around which each group is centered is the date associated with the fifteen day encounters in Chapter 4.

Table E.1: The encounters of Case I that are distinct by half a day and their frequency.

Encounters			Frequency
Month	Day	Year	
11	1.2	2010	12
11	1.8	2010	8
11	2.4	2010	4
11	3	2010	1
9	6.8	2011	1
9	7.4	2011	57
9	8	2011	31
9	8.6	2011	1
1	14.2	2012	3
1	14.8	2012	14
1	15.4	2012	14
1	16	2012	20
1	16.6	2012	23
1	17.2	2012	9
1	17.8	2012	11
1	18.4	2012	4
1	19	2012	2
4	16	2012	41
4	16.6	2012	59
8	24	2012	7

Continued on Next Page...

Table E.1 – Continued

Month	Day	Year	Frequency
8	24.6	2012	83
8	25.2	2012	10
12	18.2	2016	66
12	18.8	2016	34
4	11.5	2017	82
4	12.1	2017	18
7	12.6	2017	29
12	9.8	2020	25
12	10.4	2020	70
12	11	2020	5
6	9.7	2021	1
6	10.3	2021	63
6	10.9	2021	35
6	11.5	2021	1
11	1.5	2021	14
11	2.1	2021	86
9	30.2	2025	3
9	30.8	2025	97
1	16.3	2026	100
4	25.8	2026	88
4	26.3	2026	12
9	11.7	2026	2
9	12.3	2026	98
12	30.4	2030	36
12	31	2030	64
4	10	2031	50
4	10.6	2031	50
11	16.8	2034	22
11	17.4	2034	76
11	18	2034	2

Continued on Next Page. . .

Table E.1 – Continued

Month	Day	Year	Frequency
12	29.6	2034	23
12	30.2	2034	55
12	30.8	2034	22
6	2.3	2035	12
6	2.9	2035	88
10	20.4	2035	100
8	29	2039	100
12	31.1	2039	16
12	31.7	2039	63
1	1.3	2040	21
2	21.2	2040	3
2	21.8	2040	7
2	22.4	2040	8
2	22.9	2040	8
2	23.5	2040	3
2	24.1	2040	1
4	10.7	2040	25
4	11.3	2040	75

E.2   Case II

There are 44 encounters distinct by half a day. About half of these occur more than once but less than twenty times.

Case II is slightly more continuous than Case I because the ratio of encounters distinct by half a day to those distinct by fifteen days is greater for Case II.

Table E.2: The encounters of Case II that are distinct by half a day and their frequency.

Encounters			Frequency
Month	Day	Year	
9	26	2013	25
9	26.6	2013	29
9	27.1	2013	32
9	27.7	2013	13
9	28.3	2013	1
9	27.5	2014	27
9	28.1	2014	70
9	28.7	2014	3
2	9.9	2015	4
2	10.5	2015	9
2	11.1	2015	6
2	11.7	2015	8
2	12.3	2015	7
2	12.9	2015	5
2	13.5	2015	11
2	14	2015	5
2	14.6	2015	10
2	15.2	2015	5
2	15.8	2015	13
2	16.4	2015	11
2	17	2015	5
2	17.6	2015	1
11	27.5	2015	2
11	28.1	2015	24
11	28.7	2015	28
11	29.3	2015	28
11	29.9	2015	17

Continued on Next Page...

Table E.2 – Continued

Month	Day	Year	Frequency
11	30.5	2015	1
2	29.3	2016	33
2	29.8	2016	67
9	19.2	2030	49
9	19.8	2030	49
9	20.4	2030	2
1	29	2031	8
1	29.6	2031	64
1	30.2	2031	28
10	12.3	2031	16
10	12.9	2031	72
10	13.5	2031	12
3	8.9	2032	100
12	11.1	2032	47
12	11.7	2032	53
3	4.5	2033	41
3	5.1	2033	59

E.3 Case III

There are 172 encounters that are distinct by half a day. The majority occur more than once but less than twenty times in the 100 runs. Case III is by far the most continuous case.

Table E.3: The encounters of Case III that are distinct by half a day and their frequency.

Encounters			Frequency	Encounters			Frequency
Month	Day	Year		Month	Day	Year	
9	2.2	2010	5	12	12.9	2010	3
9	2.8	2010	15	12	13.5	2010	7
9	3.4	2010	26	12	14	2010	2
9	4	2010	24	12	14.6	2010	3
9	4.6	2010	30	12	15.2	2010	2
12	2.8	2010	1	2	18.2	2021	34
12	3.4	2010	6	2	18.8	2021	43
12	4	2010	2	2	19.4	2021	23
12	4.6	2010	5	4	14.3	2021	4
12	5.2	2010	5	4	14.9	2021	4
12	5.8	2010	7	4	15.4	2021	5
12	6.3	2010	6	4	16	2021	7
12	6.9	2010	9	4	16.6	2021	9
12	7.5	2010	8	4	17.2	2021	7
12	8.1	2010	8	4	17.8	2021	11
12	8.7	2010	4	4	18.4	2021	8
12	9.3	2010	6	4	19	2021	7
12	9.9	2010	2	4	19.6	2021	10
12	10.5	2010	4	4	20.2	2021	12
12	11.1	2010	6	4	20.8	2021	8
12	11.7	2010	2	4	21.4	2021	2
12	12.3	2010	2	4	22	2021	1

Continued on Next Column. . .   Continued on Next Page. . .

Table E.3 – Continued

Month	Day	Year	Frequency	Month	Day	Year	Frequency
4	22.6	2021	4	5	7.4	2022	3
4	23.1	2021	1	9	24.3	2022	6
5	9.9	2021	6	9	24.9	2022	24
5	10.5	2021	11	9	25.4	2022	23
11	14	2021	2	9	26	2022	22
11	14.6	2021	2	9	26.6	2022	19
11	15.1	2021	2	9	27.2	2022	3
11	15.7	2021	4	9	27.8	2022	3
11	16.3	2021	4	2	25	2023	7
11	16.9	2021	3	2	25.6	2023	28
11	17.5	2021	4	2	26.2	2023	31
11	18.1	2021	5	2	26.7	2023	22
11	18.7	2021	3	2	27.3	2023	12
11	19.3	2021	6	9	8.7	2023	4
11	19.9	2021	6	9	9.3	2023	7
11	20.5	2021	2	9	9.9	2023	18
11	21.1	2021	1	9	10.5	2023	14
12	13.2	2021	2	9	11	2023	11
12	13.7	2021	33	9	11.6	2023	14
12	14.3	2021	3	9	12.2	2023	7
5	1.4	2022	2	9	12.8	2023	6
5	2	2022	5	9	13.4	2023	3
5	2.6	2022	16	9	14	2023	4
5	3.2	2022	17	9	14.6	2023	5
5	3.8	2022	20	9	15.2	2023	4
5	4.4	2022	16	9	15.8	2023	2
5	5	2022	10	9	16.4	2023	1
5	5.6	2022	6	12	2.7	2023	5
5	6.2	2022	4	12	3.3	2023	14
5	6.8	2022	1	12	3.9	2023	24

Table E.3 – Continued

Month	Day	Year	Frequency	Month	Day	Year	Frequency
12	4.5	2023	29	11	1.4	2034	12
12	5.1	2023	23	11	2	2034	13
12	5.7	2023	5	11	2.6	2034	10
1	20.7	2034	17	11	3.2	2034	6
1	21.3	2034	21	4	17.5	2035	5
1	21.9	2034	38	4	18.1	2035	14
1	22.5	2034	23	4	18.7	2035	20
1	23.1	2034	1	4	19.3	2035	13
4	14.2	2034	2	4	19.9	2035	13
4	14.8	2034	2	4	20.5	2035	13
4	15.4	2034	2	4	21.1	2035	11
4	16	2034	1	4	21.7	2035	5
4	16.6	2034	2	4	22.3	2035	2
4	17.1	2034	1	4	22.9	2035	2
5	9.8	2034	1	4	23.5	2035	2
5	10.4	2034	13	9	11.7	2035	3
5	11	2034	29	9	12.3	2035	9
5	11.6	2034	21	9	12.9	2035	30
5	12.2	2034	21	9	13.5	2035	25
5	12.8	2034	9	9	14.1	2035	19
5	13.4	2034	4	9	14.7	2035	8
5	14	2034	1	9	15.3	2035	2
10	27.7	2034	3	9	15.9	2035	4
10	28.3	2034	3	1	28.7	2036	53
10	28.9	2034	3	1	29.2	2036	46
10	29.5	2034	8	1	29.8	2036	1
10	30.1	2034	13	9	13.9	2036	8
10	30.7	2034	5	9	14.5	2036	24
10	31.3	2034	15	9	15.1	2036	33
10	31.8	2034	9	9	15.7	2036	29

Continued on Next Column. . .   Continued on Next Page. . .

Table E.3 – Continued

Month	Day	Year	Frequency	Month	Day	Year	Frequency
9	16.3	2036	6				
10	23.2	2036	1				
10	23.8	2036	11				
10	24.4	2036	17				
10	25	2036	20				
10	25.6	2036	17				
10	26.1	2036	32				
10	26.7	2036	2				

Bibliography

[1] GIORGINI, J. "Solar System Dynamics Group, Horizons Online Ephemeris System," in *http://ssd.jpl.nasa.gov/?horizons*, date cited: 3 February 2011.

[2] TAGLIAFERRI, E., R. SPALDING, C. JACOBS, S. P. WORDEN, and A. ERLICH (1994) "Detection of Meteoroid Impacts by Optical Sensors in Earth Orbit," in *Hazards Due to Comets and Asteroids* (T. Gehrels, ed.), University of Arizona Press, Tucson, pp. 199–220.

[3] LEWIS, J. S. (2000) *Comet and Asteroid Impact Hazards on a Populated Earth: Computer Modeling*, pp. 28, Academic Press, San Diego, CA.

[4] WIE, B. (2005) "Solar Sailing Kinetic Energy Interceptor (KEI) Mission for Impacting/Deflecting Near Earth Asteroids," in *41st AIAA Joint Propulsion Conference, Tucson, AZ, July 10-13*, AIAA-2005-3725.

[5] "NASA: Near Earth Object Program," in *http://neo.jpl.nasa.gov/neo/*, date cited: 3 February 2011.

[6] MORRISON, D. (2004) "Asteroid and Comet Impact Hazards," in *http://impact.arc.nasa.gov/index.cfm*, date cited: 5 September 2010.

[7] YEOMANS, D. K. and G. H. STOKES (2003) *Study to Determine the Feasibility of Extending the Search for Near-Earth Objects to Smaller Limiting Diameters*, *Tech. rep.*, NASA: Office of Space Science Solar System Exploration Division.

[8] MARCUS, R., H. J. MELOSH, and G. COLLINS "Earth Impact Effects Program," in *http://impact.ese.ic.ac.uk/ImpactEffects/*, date cited: 15 October 2010.

[9] BRITT, R. (2002) "Evidence for Ancient Bombardment of Earth," in *http://www.space.com/scienceastronomy/planetearth/earth_bombarded_020724.html*, date cited: 15 October 2010.

[10] KOEBERL, C. (2003) "The Late Heavy Bombardment in the Inner Solar System - Is there any Connection to the Kuiper Belt Objects?" *Earth Moon Planets*, **92**, pp. 79–87.

[11] "Earth Impact Database," in *http://www.passc.net/EarthImpactDatabase/Diametersort.html*, date cited: 5 September 2010.

[12] HETHERINGTON, R. and R. G. B. REID (2010) *The Climate Connection - climate change and modern Human Evolution*, Cambridge University Press, Cambridge UK.

[13] "NASA Picture of the Day," in *http://apod.nasa.gov/apod/ap071114.html*, date cited: 6 September 2010.

[14] LAKDAWALLA, E. (2008) "The Full Story of Earth-Impacting Asteroid 2008 TC3," in *http://www.planetary.org/blog/article/00001684/*, date cited: 5 September 2010.

[15] HAMILTON, C. "Comet Shoemaker-Levy 9," in *http://www.solarviews.com/eng/levy.htm*, date cited: 15 October 2010.

[16] NAKAMURA, T. and H. KURAHASH (1998) "Collisional Probability of Periodic Comets with the Terrestrial Planets: an Invalid Case of Analytic Formulation," *The Astronomical Journal*, **115**, p. 848.

[17] MILANI, A., M. E. SANSATURIO, G. TOMMEI, O. ARRATIA, and S. R. CHESLEY (2005) "Multiple Solutions for Asteroid Orbits: Computational Procedure and Applications," *Astronomy and Astrophysics*, **431**, pp. 729–746.

[18] MILANI, A. (1999) "The Asteroid Identification Problem I: Recovery of lost asteroids," *Icarus*, **137**, pp. 269–292.

[19] MILANI, A., S. R. CHESLEY, M. E. SANSATURIO, G. TOMMEI, and G. B. VASECCHI (2005) "Nonlinear Impact Monitoring: Line of Variation Searches for Impactors," *Icarus*, **173**(2), pp. 362–384.

[20] CHAN, F. K. (2008) *Spacecraft Collision Probability*, The Aerospace Press, El Segundo, CA.

[21] KLINKRAD, H. (2006) *Space Debris: Models of Risk Analysis*, pp. 222-226, Praxis Publishing, Ltd., Chichester, UK.

[22] WIESEL, W. E. (1989) *Spacecraft Dynamics*, pp. 278-281, 2nd ed., McGraw-Hill.

[23] CHODAS, P. W. and D. K. YEOMANS (1999) "Orbit Determination and Estimation of Impact Probability for Near Earth Objects," in *Rocky Mountain Guidance and Control Conference, Breckenridge, CO, Feburary 3-7*, AAS 99-002, pp. 21–40.

[24] "NEODyS," in *http://newton.dm.unipi.it/neodys/*, date cited: 21 January 2011.

[25] NEWHALL, E. M. STANDISH, JR., and J. G. WILLIAMS (1983) "DE102: A Numerically Integrated Ephemeris of the Moon and Planets Spanning Forty-four Centuries," *Astronomy and Astrophysics*, **125**, pp. 150–167.

[26] HOWELL, K. (1983) *Three-Dimensional, Periodic Halo Orbits in the Restricted Three-Body Problem*, Ph.D. dissertation, Stanford University.

[27] TAPLEY, B. D., B. E. SHULTZ, and G. H. BORN (2004) *Statistical Orbit Determination*, Elsevier Academic Press, Burlington, MA.

[28] CHESLEY, S. R. (2005) "Potential Impact Detection for Near-Earth Asteroids: The Case of 99942 Apophis (2004 MN_4)," in *Proceedings of the International Astronomical Union*, vol. 1, pp. 215–228.

[29] MILANI, A., S. R. CHESLEY, M. E. SANSATURIO, F. BERNARDI, G. B. VASECCHI, and O. ARRATIA (2009) "Long Term Impact Risk for (101955) 1999 RQ_{36}," *Icarus*, **203**, pp. 460–471.

[30] CHESLEY, S. R. and A. MILANI (1999) "Nonlinear Methods for Propagation of Orbital Uncertainty," in *Astrodynamics Conference, Girwood, AK, August 16-19*, AAS 99-418, pp. 1857–1870.

[31] SOFTWARE *MATLAB*, ©The MathWorks Inc., various ed.

[32] DER, G. and R. DANCHICK (1996) "Analytic and Numerical Error Covariance Matrix Propagation (for Spacecraft in Earth Orbital Environments)," in *Astrodynamics Conference, San Diego, CA, July 29-31*, AIAA Paper 96-3661, pp. 854–878.

[33] CHAN, F. K. (2010) "The Limitations of Approximating a 'Smooth' Curve by a Straight Line," *unpublished work*, The Aerospace Corporation.

[34] ALFANO, S. and M. GREER (2003) "Determining If Two Solid Ellipsoids Intersect," *Journal of Guidance, Control and Dynamics*, **26**(1), pp. 106–110.

[35] CHAN, F. K. (2002) "A Simple Mathematical Approach for Determining Intersection of Quadratic Surfaces," *Advances in Astronautical Sciences*, **109**, pp. 785–801.